Univerzita Karlova v Praze

Matematicko-fyzikální fakulta

DIPLOMOVÁ PRÁCE

Orsolya Molnárová

Studium nestabilní plastické deformace metodou akustické emise

Katedra fyziky materiálů

Vedoucí diplomové práce: Ing. Patrik Dobroň, Ph.D.

Studijní program: Fyzika

Studijní obor: FKSM

Praha 2014

I would like to express my gratitude to my supervisor Ing. Patrik Dobroň, Ph.D. for his guidance, sustain and good advices. My thanks must also go to doc. RNDr. František Chmelík, CSc, who, in spite of having practically no free time, still managed to find some time to provide help and advice. I also thank very much to Ing. Jana Kálalová and Marta Čepová for their help during experimental work. Last but not the least important, I owe more than tanks to my family members for their financial support and encouragement throughout my life. Without their support it would be impossible to finish my studies and graduate seamlessly.

This wok was completed within the framewok of the research grant P10811/1267 by the Czech Science Foundation.

I declare that I carried out this master thesis independently, and only with the cited sources, literature and other professional sources.

I understand that my work relates to the rights and obligations under the Act No. 121/2000 Coll., the Copyright Act, as amended, in particular the fact that the Charles University in Prague has the right to conclude a license agreement on the use of this work as a school work pursuant to Section 60 paragraph 1 of the Copyright Act.

In…..... date..... signature

Název práce: Studium nestabilní plastické deformace metodou akustické emise

Autor: Orsolya Molnárová

Katedra / Ústav: Katedra fyziky materiálů

Vedoucí diplomové práce: Ing. Patrik Dobroň Ph.D., Katedra fyziky materiálů

Abstrakt: Byl studován výskyt plastických nestabilit v protlačované slitině AlSi1MgMn (6082) a válcované slitině AlMg4.5Mn0.4 (5182) jako důsledek změny rychlosti deformace a tepelného zpracování. Vzorky byly podrobeny jednoosé deformaci s různou rychlostí za pokojové teploty (RT). Výsledky jsou doplněny *in situ* detekcí akustické emise (AE) a parametry AE jsou korelovány s mikrostrukturou a deformačními křivkami. Všechny vzorky vykazovaly Portevin-Le Châtelierův (PLC) efekt různých typů, v závislosti na tepelném zpracování a rychlosti deformace. Výskyt PLC efektu se projevuje nespojitými signály AE s vysokou amplitudou. Statistická analýza ukázala mocninný charakter distribucí pravděpodobnosti signálů AE.

Klíčová slova: plastická nestabilita, akustická emise, samoorganizovaná kritičnost

Title: Investigation of plastic deformation instabilities by the acoustic emission technique

Author: Orsolya Molnárová

Department / Institute: Department of Physics of Materials

Supervisor of the master thesis: Ing. Patrik Dobroň, Ph.D., Department of Physics of Materials

Abstract: The influence of the strain rate and heat treatment on the occurrence of plastic instabilities in extruded AlSi1MgMn (6082) and cold rolled AlMg4.5Mn0.4 (5182) alloys was studied. The samples were uniaxially loaded at various strain rates and at room temperature (RT). The results are discussed using concurrent acoustic emission (AE) monitoring during mechanical testing and the AE parameters are correlated to the microstructure and to the stress-time curves. All samples exhibited the Portevin-Le Châtelier (PLC) effect of different types, dependently on the heat treatment and the applied strain rate. The occurrence of the

PLC effect is manifested by burst AE signals with high amplitudes. Statistical analysis of the AE signals has shown the power-law probability distribution.

Keywords: plastic instability, acoustic emission, self-organized criticality

Contents

Introduction

The continuously developing world industry, as a consequence of the growing natural resource's scarcity, has to face the problem of the limited resources and thus it has to improve the material and energy efficiency. Therefore, its ultimate goal is to reduce the environmental impacts associated with the processing and use of materials. It refers to the reduction of the energy used during the production or the products service and to create long-life products. Due to the resource scarcity threat, recycling is of an even higher importance. It spares raw material and saves on additional energy. In most cases, the energy used for renewing a material is much less than the production energy of the raw material.

The above mentioned requirements can be fulfilled using lightweight metallic materials with the appropriate properties. One of the convenient materials is aluminium (Al). It has a low density, belongs to oxidation resistant materials, its alloys show high strength and therefore they can be utilized in long-life applications. This metal is highly suitable for recycling because it requires only 5% of the energy of primary Al production [1].

Its excellent strength to weight ratio offers chances to be widely utilized in the manufacture of transport equipment and engineering structures. The car industry is encouraged to use the Al alloys to make an economical vehicle. The first car whose whole body was made of Al alloys is the Audi A8 [2]. Today about 110-145 kg of Al alloys are used in production of a car and this amount grows with every year. A car with components made of Al alloys can be 24% lighter than that with components made of steel and therefore a fuel consumption is reduced by 2 litres on 100 km. Al alloys, due to the possible weight reduction of the product, are frequently used in the aircraft industry as well.

In spite of their great properties, a number of industrially important Al alloys may exhibit plastic instability under certain conditions. To improve the reliability of the machine parts produced from these alloys, it is required to understand these processes which can occur during their fabrication and service, thus deteriorating their performance.

The structural defects of materials can be detected by a number of methods such as the techniques using the X-rays, neutrons, the eddy currents etc. One of the non-destructive evaluation methods is the acoustic emission (AE) technique, based

on the detection of elastic waves, which are generated within the material by a rapid release of energy as the result of irreversible changes in the material structure. AE is also *in-situ* method which offers real time information about the evolution of the dynamic state of the material. AE can be used in defectoscopy and in monitoring of engineering structures, where it is capable of detecting of damage processes before they become of critical character.

One of the most spectacular phenomena, occurring during plastic deformation of some alloys processed at certain conditions, is the unstable plastic flow so called Portevin- Le Châtelier (PLC) effect. It is characterized as a macroscopic spatio-temporal instability of plastic deformation and it can negatively affect mechanical properties of structural materials. When PLC effect is combined with the embrittlement by environmental conditions [3] − like the intergranular corrosion, it can lead to failure of the whole component built from such a material [4]. Therefore, the investigation of the plastic instabilities like PLC effect is of a high importance.

1. Theory

1.1. Aluminium and its alloys

Aluminium (Al) is the third most abundant element in the Earth's crust (only silicon and oxygen are more plentiful) and constitutes about 8% of its weight [5]. Thanks to its unique properties, Al is nowadays the second most commonly used metal and it is called the metal of the Third Millennium.

Because of its high chemical activity, Al never occurs in its metallic form in the nature, but it is present almost in all rocks, plants and animals. The main ore of Al is bauxite - a mixture of hydrated aluminium oxides with oxides of iron, titanium and silicon. With refinement the bauxite in the Bayer process, aluminium oxide also known as alumina (Al_2O_3) is obtained. In this process, the grinded bauxite is digested with a hot solution of sodium hydroxide (NaOH). This solution is refined by filtering off impurities, called as red mug. Due to cooling, the alkaline ($NaAl(OH)_4$) aluminium hydroxide precipitates ($Al(OH)_3$), which is after the reheating decomposed to aluminium oxide and water vapour [1]. The final stage is the reduction of Al through the Hall-Heroult process, where the alumina is electrolyzed in molten cryolit (Na_3AlF_6) at 950 ˚C [1].

The production of Al from bauxite requires high gravity of raw material and energy, e.g. for the production of a ton of Al, four tons of bauxite is needed. This is the main justification for Al recycling, which needs only 5% of the production’s energy of the primary Al [1].

Pure Al is soft, ductile, has a low density, which is about one-third of the density of iron or copper. Al crystallizes in the face-centered cubic (fcc) lattice, which is stable from 4 K to its melting point (660˚C) [6]. It is an excellent conductor of heat and electricity. The pure Al is highly chemically active and it reacts with the atmospheric oxygen to form a non-conducting aluminium-oxide (Al_2O_3) film, which protects the material from further corrosion [6].

Although most metallic elements readily alloy with aluminium, only a few form important commercial aluminium alloys. These elements serve to improve alloy properties and characteristics. None of these elements is completely miscible with Al in solid state. Zinc has the greatest solubility in Al and some others like Ag, Mg, Li have solid solubility greater than 10 at.% [6].

The wrought Al alloys can be classified according to EN 573-1 into 9 groups with respect to alloying elements [7]. These groups with their characteristic properties [6, 8] are summarized in Table 1.

Code of the series	**Major alloying element**	**Characteristic properties**
1000	Al min. purity 99.00%	high conductivity
2000	Cu	strong, hard
3000	Mn	strong
4000	Si	high wear resistance
5000	Mg	great corrosion resistance
6000	Mg a Si	middle strong
7000	Zn	with Mg is the strongest alloy
8000	other elements	
9000	unused group	

Table 1: Groups of the wrought Al alloys according to the major alloying elements and their characteristic properties

The alloys AlMgSi belong to the group 6000. It is a class of heat treatable alloys, which is used for wrought and casting products as well. They have a number of favourable properties like high strength, low quench sensitivity and good corrosion resistance [6]. This group contains Mg and Si as major addition elements and metals like Fe and Mn are always present in alloys as impurities. In dependence of the alloys exact composition and the solidification conditions of the cast 6000 alloys, a wide range of intermetallic phases may be formed. Their volume fraction, morphology and composition can significantly influence the final physical properties of the alloy. When the alloys of the group contain enough magnesium and up to 12% silicon magnesium silicide (Mg_2Si) precipitates, which make the material heat treatable. Si also improves the corrosion resistance and the fluidity of the molten material. More than 13% Si reduces the machinability [6, 8]. The 6000 Al alloys are frequently used for machined products usually after alloying with elements of low melting point like lead or bismuth.

The minor alloying components of the group 6000 are Ca, Cr, Mn, Pb and Bi. With addition of Ca to a 6000 alloy, $CaSi_2$ forms, which slightly increases the electrical conductivity. Cr has a slow diffusion rate and can form finely dispersed

phases which hinder the nucleation and the grain growth during heat treatment. Disadvantage of the alloying by Cr is that it increases the quench sensitivity when the hardening phase precipitates on the Cr-phase particles. Pb is a toxic element, whose application in automotive and electronic industry is restricted by law to a maximum value of 0.4%. Pb. Also Bi forms a low-melting phase in the material and promotes chip breaking [6].

The 6082 alloy is also denoted as EN AW-6082 or EN AW-Al Si1MgMn [9]. This alloy has a very good corrosion resistance, a good weldability and machinability. In T4 condition, after a stabilizing heat treatment, it has a good cold formability. A high Mn addition can control the grain size of the alloy what results in its high strength. The most common intermetallic phases present in 6082 alloy are ß-Al_5FeSi, α-$Al_{15}(FeMn)_3Si$, Al_9Mn_3Si, α-$Al_{12}Fe3Si$, Mg_2Si [10]. The alloy is used especially in heavy duty structures such as in ship building, truck frames, bicycles and rail coaches etc.

The 5182 alloy is also denoted as EN AW-5182 or EN AW-AlMg4.5Mn0.4 [9]. AlMg alloys belong to the non-heat treatable alloys; however Mg does provide substantial strengthening and good ductility after cold work. Although Mg is largely present in solid solution, it can also appear as eutectic Mg_2Al_3 dependently on alloy's content. This element with Si can form Mg_2Si. Cr and Mn, as an additive, form fine dispersoid particles and therefore they serve as grain refiner [6]. This alloy has an excellent corrosion resistance, unless the material is held at elevated temperatures for long time period. Due to good formability, the alloy is used for manufacturing the easy-open ends of beverage cans or in the automotive industry.

1.2. Plastic deformation

1.2.1. Dislocations and their interaction

Dislocations are line defects in the crystal lattice having a strain field around. These defects can glide along specific slip planes in the slip direction, climb and organize themselves into pile-ups and dislocation walls. Through their strain field, they can interact (stop, multiply and annihilate) with each other or with other defects in crystal lattice (foreign atoms, precipitates etc…). A dislocation is characterized by its line element ($\vec{\xi}$) and the Burgers vector ($\vec{b}$). According to their mutual orientation

screw ($\vec{\xi} \parallel \vec{b}$) and edge dislocations ($\vec{\xi} \perp \vec{b}$) exist [11]. In real materials, mixed dislocations with both screw and edge components occur. The dislocation glide occurs due to the rearrangement of atoms in the core and consequently glide is a conservative motion. Unlike glide, climb is a non-conservative motion and it is realized through the movement of point defects.

The dislocations can decompose into partial dislocations if the sum of the energy of the partials is less than that of the original dislocation. The area they border after decomposing is the stacking fault. The partial dislocations can be glissile, when the Burgers vectors of the partial dislocations lie in the slip plane (Shockley type) or sessile, when they does not (Frank type). These partial dislocations can interact: in fcc systems, the interaction of two Shockley type partial dislocations may create a Lomer-Cotrell dislocation, which is immobile [11]. The total structure, the Lomer-Cotrell dislocation and the two stacking faults which are bordered on the other side by Shockley partial dislocation, is called a stair-rod dislocation. Lomer-Cotrell dislocation can combine (possible due to the moving Shockley partials) to form a stacking fault tetrahedron.

In most crystalline materials, the dislocation density increases quickly during plastic deformation, which leads to work hardening. Dislocations are produced as a consequence of the local overstress around the dislocations. The most widely known sources of dislocations are the Frank-Read sources and the double-cross slip [11, 12].

The macroscopic measurable quantities that describe features of plastic deformation like stress, strain etc. cannot be taken as the result of motion of single dislocations. Just when the mutual dislocation interaction can be neglected, i.e. the dislocation density is not high or the plastic strain is small, the response can be considered as the sum of uncorrelated events [12]. However, during plastic deformation, the dislocation density reaches a point, when the dislocation-dislocation interaction cannot be neglected. Atomistic methods were used to study this interaction mechanism, but they cannot fully describe the long-range character of the stress fields. Because of this complexity, there exists a gap in the theory. The dislocation dynamics is not yet fully developed, but there exist simulations of the collective behaviour of dislocations.

Although the dynamics of the dislocation system is hard to be described, the statistics performed on experimental data can uncover information about the

behaviour of dislocations as a spatially distributed nonlinear dynamic system. Recent analyses of deformation curves are realized using methods of the theory of non-linear dynamical systems in order to find a dynamical model [12], which can describe the serration's structure on deformation curve.

1.2.2. Plastic deformation of polycrystals

Crystals are solid materials consisting of atoms arranged according to a defined repeated three dimensional pattern. In single crystals, the crystal lattice is continuous and unbroken for the whole sample. The symmetry of the unit cell is decisive for the physical properties. Most solid materials found in the nature appear polycrystalline form. They are composed of randomly oriented crystalline regions, grains.

Deformation is a physical process during which the shape or size of the body alters in accord with the applied mechanical force. Most solids initially deform elastically, which means that they can return to their original shape. From a certain critical point (the limit of the elastic deformation − the yield point) [11], the material rearranges its internal structure and this plastic deformation is irreversible.

The stress necessary for plastic deformation of polycrystals is higher than in the case of the single crystals because of the different orientation of the grains. For single crystals, the critical resolved shear stress (CRSS, τ_0) determines the stress necessary to initiate a slip in a certain slip system. The shear stress for polycrystalline materials is replaced by the offset yield strength – the strength at a strain of 0,2 ($\sigma_{0,2}$) [11]. During deformation of some materials, it can be observed that after reaching an upper yield point the stress drops quickly to a lower yield point. If the metal has both yield points, Lüder bands can develop [12].

Plastic deformation of a single crystal is produced by movement of dislocations and/or by twinning. The plastic deformation of polycrystals cannot be described as the deformation of a group of single crystals, because it is highly influenced by the grain boundaries and by the orientation of the grains [12]. Deformation of a polycrystal starts in those grains, which have slip planes favourable oriented to the applied stress.

The stress-strain curve can be characterized by:

- extension (ε)- the relative elongation of the measured specimen in percent

- offset yield strength ($\sigma_{0,2}$)- after reaching this point the plastic deformation of the material starts

- yield strength (σ_y)- the stress corresponding to a certain (y) extension of the specimen

- ultimate strength (σ_m)- the maximum stress that the material can withstand before failure

The major difficulty by a theoretical description of plastic deformation is the fact that such a process is highly dissipative and irreversible. It means that during the process about 90 % of the energy turn into heat and there is no theoretical framework which deals with so high dissipation [12]. The system of dislocations during the deformation is very far from equilibrium, where nonlinearities have a significant role. In the past decades, the nonlinear dynamics was developed, but anyway there still are not any acceptable frameworks which can statistically describe this mechanism. Other complications originate from the fact that the dislocations can be activated thermally and athermally. The plastic deformation is usually inhomogeneous, especially at high strains. To solve the difficulty, statistical and dynamical methods like the distribution function theoretic approach or the reductive perturbative technique were developed to analyse the experimental data [12].

1.2.3. The Portevin-Le Châtelierier effect

One of the most interesting phenomena, occurring during deformation tests of some alloys deformed over a certain range of temperatures and at an appropriate strain rate, is a kind of unstable plastic flow, so called Portevin- Le Châtelier (PLC) phenomenon, which is characterised as a macroscopic spatio-temporal instability of plastic deformation, and manifests by serrations on the stress-strain curve (jerky flow).

This effect was firstly described by F. Le Châtelier in 1909 and thereafter it was studied by M. Portevin and F. Le Châtelier in 1923 [12]. Investigations of this effect has started with conventional strain- and stress-controlled tensile tests. During the years, measuring methods have been improved and now there is a deal of modern methods for the investigation of the PLC effect such as optical, acoustic, mechanical or electromagnetic methods [3].

The most widely accepted explanation of the PLC effect is based on interaction between the moving dislocations and the diffusing atoms which is known as dynamic strain aging (DSA). Because these mobile atoms are impurities or atoms which are not in their lattice points, a stress field appears around them. This stress field interacts with the stress field of the dislocations which leads to a stress driven diffusion of mobile atoms to the dislocation core. Therefore, when the dislocations during their motion are temporarily pinned at obstacles (crystal defects), solutes diffuse either by volume or pipe diffusion around the stopped dislocations which leads to strengthening. As loading of the specimen proceeds, the so far locked dislocations will abruptly breakaway from the obstacles and move until they are again stopped. When the dislocations and the mobile solute atoms have almost the same velocity, the process repeats [13]. It manifests by movement of deformation bands on macroscopic scale, also observable as serrations on deformation curve (PLC effect) [14].

With increasing strain rate at a constant temperature the waiting time of dislocations at obstacles decreases, the stress needed for unpinning decreases. At constant strain rate but decreasing temperature the time while the solute atoms diffuse to the dislocations increases. The PLC instability demonstrates, in a certain range of strain rates and temperatures, where the two time scales are of the same magnitude. This competition between the slow aging and rapid unpinning of dislocations leads to the negative strain rate sensitivity (SRS) of the flow stress [12].

The DSA is responsible for a plateau or for a peak in flow stress and it also affects the work hardening and changes the ductility with temperature [15].

The PLC effect starts at a certain critical strain, when the strain rate sensitivity becomes negative [16] and the inhomogeneous deformation begins. The critical strain is highly strain rate and temperature dependent. In substitutional alloys, the process is supported by vacancies and the high density of the dislocations, while in interstitial alloys it is influenced only by the mobile dislocation density [12].

A characteristic macroscopic feature of PLC effect is the localization of strain in form of deformation bands and their motion with the increasing stress. These bands are just a few millimetres thick and are inclined at about 55° to the deformation axis [3]. The avalanches of dislocations within the bands are reflected on the stress-time curves as stress drops.

Experiments showed different types of the propagation of PLC bands, assigned as types A, B and C, some researchers have added also a D and E band type [17, 18]. They appear at different temperatures and strain rates. The grain size, the precipitates and the preparation of the surface also influence the occurrence of the band types. They have different spatial arrangement and specific appearance on deformation curves. In the case of type A, the bands appear at the end of the specimen gauge and propagate quasicontinuously along the gauge. This type of bands cause irregularly shaped and very small stress drops on deformation curve, which initially rise above the normal stress level. Type B has a hopping character as a result of the band jumping along the gauge. The drops on deformation curves have a slightly irregular character [3]. The serration fluctuates about the stress-strain curve. For type C, bands are randomly nucleated at different places of the specimen gauge but the analysis of the serrations shows some correlation [19, 20]. The deformation curve is characteristic of serrations of a certain amplitude and frequency. The drops fluctuate below the normal stress level. Type D exhibits plateaus on the σ–ε curve, which is caused by the propagation of dislocation bands without strain hardening ahead of the moving band. Type E serration generally appears at high strains. This serration type is similar to type A serration, but with little or no strain hardening during band propagation. The E type is often preceded by type A serration [17, 18, 21].

The strain rate and temperature influence the time needed for the dislocation to overcome the hindering obstacles. It means that the critical stress will decrease with increasing strain rate, but it also affects the bands speed. Usually, higher strain rate is connected with the A type and the lowest with the C type bands. The B bands emerge at an intermediate level [12]. With respect to experiments, it is known that at higher temperatures the C bands occur and with decreasing temperature the band type changes into type B after that into type A.

The grain size also influences the appearance and character of the PLC effect. The critical strain is higher in a material with larger grains and the amplitude of the stress drops is larger in a material with finer grain size [22]. Anyway, the grain size does not have any distinctive effect on the band velocity and on the band width [12]. The precipitates hinder the PLC effect; they cause inverse behaviour and change the effect of the temperature and strain rate on the material [23]. The surface preparation also can affect the PLC effect. Deformation bands can propagate faster in polished

specimen, while on a rough surface more nucleation points appear which produce stress rise creating deformation bands [24]. The thickness, strain and velocity of deformation band increases with increasing strain rate. The volume of specimen has no effect on velocity or strain of deformation band, but the thickness of band increases with increasing volume [12].

Deformation tests, combined with the laser scanning extensometry technique, have shown that after the stop of the B bands, new bands are nucleated and moveto the opposite direction with the opposite inclination. Another observation is that some bands can split to two bands with different orientation and move to the opposite directions [3].

The PLC effect occurs in some industrially important alloys like mild steel and Al, Cu or Zr alloys [3] and is responsible for the degradation of their properties. The surface of products made from such alloys can become rough, during their use defects in the structure can emerge. This affects the mechanical properties of material, especially increases the flow stress, hardening rate and embrittlement and decreases the ductility, fracture toughness and strain rate sensitivity [3]. As a consequence of these changes the material can become susceptible to failures and the part can easily fail [4].

1.3. Acoustic emission

1.3.1. Description of the acoustic emission

Acoustic emission (AE) is transient elastic waves, which are generated by sudden release of energy from localized sources within the material. The term of acoustic emission is also used for the non-destructive method which is based on this effect [25].

The AE method is used for detection of dynamic changes in materials structure and provides information from entire volume in real time (*in-situ* measurement). With using at least three sensors, the location of the AE sources can be done. The AE method can be easily used for monitoring of constructions. Disadvantage of the AE method is given by a complex character of AE signals (wave packet) resulting in loss of some information about the AE. Furthermore, the low energy AE signals can be filtered out together with noise [25, 26].

The AE method has a long history. Already about 6500 BC sounds generated by the cooling of glass, metals or porcelain were observed. Audible AE was also observed during earthquakes or from cracking of ice on a lake.

The first written record of AE dates back to the 8. Century. It comes from Jabir ibn Hayyan, who wrote about the sound produced during the deformation of tin [27]. Beginning of modern history of AE is connected with Joseph Kaiser, who described the phenomenon of AE in his dissertation [28]. Since then, the AE technique has developed to one of the most important tools in materials research.

The most important sources of AE are the initiation and growth of cracks, dislocation movements [29], twinning and the phase transformations. In all cases, the AE originates from the relaxation of stress fields associated with the defect motion.

The three main dislocation processes which produce AE are:

- relaxation of stress field caused by the passage of dislocations
- annihilation of dislocations
- acoustic radiation of accelerated (deccelerated) dislocations

The resulting AE signal is not only determined by the source parameters but also by the propagation and detection of AE waves and processing of the AE signals. During propagation, the wave packets interact with the material. As a consequence it will be a damped wave with a changed shape, which includes information about the source and the discontinuities in the material. AE waves produce surface displacement which can be detected by piezoelectric detectors. [25].

Scruby et al. [30] derived the formula for the maximum amplitude ΔU of the surface displacement of the material in the epicentre. The epicentre is the point, where the wave first arrives at the surface of the specimen. In their model the AE originates from the growth of n dislocation loops with a v velocity of growth to the final radius a. The loops are inclined at 45° and they are located in an r depth under the epicentre. The formula:

$$\Delta U = \frac{nbavc_T^2}{rc_L^3}, \qquad (1)$$

where b is the Burgers vector, c_L and c_T are the velocities of longitudinal and the transversal waves.

According to this formula it can be estimated that for a measureable AE in polycrystalline Al alloys with an average grain size of 80 μm, the collective motion of at least 100 dislocations is needed [30].

1.3.2: Detection of the acoustic emission

Two kinds of AE signals can be distinguished. If the elastic waves are generated simultaneously by a large number of sources and the AE signal has a random character then it is called continuous emission. The burst emission occurs as a consequence of an instable fashion of plastic deformation or degradation of materials [20, 31].

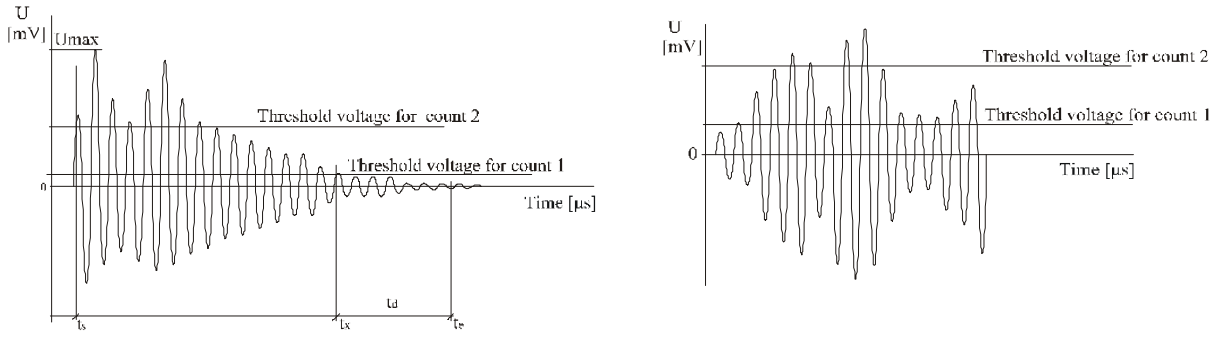

Fig.1: The burst (on the left) and the continuous AE signal

The AE is characterized by the following parameters [32]:

- Count rate – $\dot{N}_C$ – the number of the emitted pulses with an amplitude greater than the threshold
- Event rate – $\dot{N}_E$ – the number of the events during a unit time
- Cumulative AE count – N_C – the sum of counts during a period
- Cumulative AE events – N_E – the sum of events during a time period
- U_{RMS} – the root mean square of the voltage of the AE signal

$$U_{RMS}{}^2 = U_m^2 + U_n^2 - 2\gamma U_{RMS} U_n, \tag{2}$$

where U_m is the total voltage, U_n is the noise voltage. Assuming a low correlation between U_m and U_{RMS}:

$$U_{RMS}{}^2 = U_m^2 + U_n^2 \tag{3}$$

- E_{AE} – energy of the AE event

$$E_{AE} - \frac{1}{Z^2}\int_0^{t_e} U_{RMS}^2 d\tau, \tag{4}$$

where Z is the amplification of the signal

- t_s – start time of the AE event - time, when the AE signal first time exceeds the lower threshold level

- t_d − dead time − the shortest time interval between the AE events. If AE signal does not exceed the threshold level in this period, the AE event is finished.
- t_e − the time of the AE event
- A_{max} − the maximal amplitude of the AE event
- t_r − the rise time

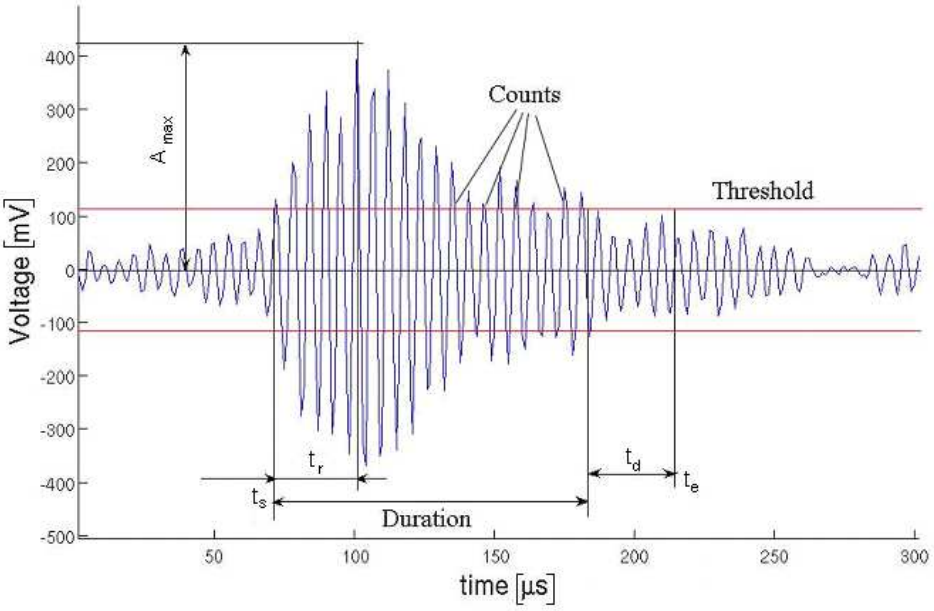

Fig.2: The parametrisation of an AE event

The AE equipment consists of sensor, preamplifier, measuring device and of computer with the corresponding program for detection and evaluation of AE signals.

The AE measurement is based on the detection of the surfaces displacements, which are produced by stress waves. The AE sensors are usually piezoelectric sensors, made from a ceramic like lead zirconate titanate (PZT), which uses the piezoelectric effect to measure the pressure and subsequently converts it in electrical voltage signal. There are two types of detectors. The resonance type detector is the most sensitive around the resonant frequency. The broad-band sensor has a flat response in wide frequency interval but is less sensitive. They normally work at frequencies between 50 kHz and 1 MHz, because lower frequencies can be disturbed by noise [26, 31].

The sensitivity of the sensor is defined as:

$$dB_{AE} = 20\, log\left(\frac{U}{U_r}\right), \tag{5}$$

where U_r is the reference voltage and it equals 1μV [25].

To keep the high ratio between AE signal and noise, a preamplifier is usually used. Amplified AE signal is filtered to eliminate low frequencies which are influenced by a noise of various nature (friction, vibrations from testing machine etc.). Thereafter, AE signal is parametrized in computer.

1.4. Self-organized criticality and power-law distribution

Recent studies have proven that PLC effect can be characterized by scale invariance through the power-law distribution of dislocation avalanches which indicates the self-organization of dislocation groups. With statistical and dynamical analyses, it was found that there are two major phenomena, i.e. the self − organized criticality (SOC) and the chaotic dynamics [20].

The self-organized criticality is the ability of the system to maintain itself after a critical point which is called the edge of the chaos. At this point a small change can push the whole system into a chaotic system or into the system of predictable behaviour.

SOC exists typically in slowly changeable non-equilibrium systems with a large degree of freedom and a high nonlinearity. The concept was published in 1987 by Bak, Tand and Wiesenfeld [33]. Thereafter, many examples controlled by SOC have been identified like epidemics or biological evolution. Also, under certain conditions, the system of dislocations is driven by SOC. The transition of the systems from the chaotic to the SOC behaviour can be studied with a wide range of analyses like the statistical, multifractal or dynamical analyses. For systems with SOC, it is typical the self-similarity and the scale independent (fractal) behaviour what means that the dynamics of the system exhibits the same structure over the scales. The mentioned analyses can uncover this correlation. The power-law distribution analysis can show, if there is a relation between the value of a property and the probability of the occurrence of such property values. The multifractal analysis can uncover the correlation between certain time or property scales [34].

The power law is a mathematical relationship between two quantities, where the frequency of an event varies as a power of one of its variable:

$$f(x) = Kx^{\alpha}, \tag{6}$$

where $x>0$, α is the scaling parameter, K is a constant [35].

The main attribute of power laws is their scale invariance. The scale invariance is a feature of laws that they do not change if scales of variables are multiplied by a common factor. Mathematically:

$$f(cx) = a(cx)^{k} = c^{k} f(x) \propto f(x). \tag{7}$$

It can be shown, that the power laws are the necessary and sufficient condition for scale free behaviour [35].

The power-law probability distribution has a density function in the form:

$$p(x) \propto L(x) \cdot x^{-\alpha}, \tag{8}$$

Where $\alpha>1$ and $L(x)$ is a slowly varying function [35]

A lot of studies report about the performed analysis on experimental data of single crystals. In these materials the only sources of dislocation avalanches are the slip and the twinning. They calculated the distribution connecting the AE energy E_{AE} with the amplitude of the acoustic events A:

$$E_{AE} \sim A^{2}. \tag{9}$$

The distributions always followed the power-law with an exponent of $\alpha = 1.5 \pm 0.1$ [36]. This statistical analysis can be performed for AE events as well as for local strain rate what indicates the avalanche-like character of the plastic flow [20].

In studies like [37] the statistical analysis of the experimental data obtained from polycrystalline materials revealed unexpected behaviour. It was shown that the statistical distribution of AE energy obeys power law and is like a general property of the intermittency of plastic flow. The power-law exponent α_{AE} altered with the chosen strain rate and it changed also during the deformation, but it was possible to find an interval within it remained unchanged. Varying exponent values can be explained by the dislocation aging, grain boundaries and by the folding of the AE signals from different sources. During the plastic flow, the value exponent changed from 2 to over 3. Below the critical strain it was lower than 2 [20].

The statistical analysis in [13] reveals different correlation regimes between the stress serrations, which also depends on the strain rate. They found the operability of the power-law statistics for the low amplitude stress serrations in AlMg and CuAl alloys [38] for the stress drop size and duration which indicates the

self-organized behaviour. For the type B deterministic chaos and a near-Gaussian distribution was found [13]. This fact demonstrates that the plastic flow is connected with the avalanche-like dislocation dynamics [39].

The power-law statistical distribution only characterizes the probability of the occurrence of a plastic event with a given energy, but it does not give information about the relative arrangement of the events. The multifractal analysis can uncover the presence of correlations and characterize the heterogeneity of the scaling properties, but does not give any information about the location of the corresponding events [13].

2. Experimental procedure

2.1. Experimental material

Measurements were performed on 6082 (AlSi1MnMg) alloy which was produced by conventional casting and afterwards extruded at 430 °C. The chemical composition of the alloy is given in Table 2 [9].

Element	Si	Fe	Cu	Mn	Mg	Cr	Zn	Ti	Other
wt%	0.7-1.3	0.5	0.1	0.4-1.0	0.6-1.2	0.25	0.2	0.1	0.15

Table 2. The chemical composition of the 6082 alloy [9]

The second investigated material was a 5182 (AlMg4.5Mn0.4) alloy which was produced by casting and cold rolling. The chemical composition of this alloy can be seen in Table 3 [9]. The basic study of plastic instabilities in this alloy has been already described in [40]. In the present work, the self-organised criticality model with power law distribution will be applied on the results obtained during the investigation of this alloy.

Element	Si	Fe	Cu	Mn	Mg	Cr	Zn	Ti	other
wt%	0.20	0.35	0.15	0.25-0.50	4.0-5.0	0.10	0.25	0.10	0.05

Table 3. The chemical composition of the 5182 alloy [9]

2.2. Methods of measurements

2.2.1. Microhardness

Microhardness measurement was used to define the hardening state of the as - received material and to determine a stress released condition of heat treated samples. To determine the nondirectionality of the results, the microhardness was measured parallel (∥) and perpendicular (⊥) to extrusion direction (ED).

A Vickers test for microhardness was performed on the microhardness tester Qness 10 A+ produced by the company Qness.

The Vickers hardness was tested by pressing a 136˚ pyramidal diamond indenter into the sample by an accurately controlled test force of 100 g. The force was maintained for 10 seconds, after that the indenter was removed, and the diagonals of the square shaped indent were measured. The hardness was computed by the formula:

$$HV = k.\frac{F}{d^2}, \quad (10)$$

where k is a constant (k =0.1891), F is the test force and d is the arithmetical average of the measured diagonals.

2.2.2. Light microscopy

Specimens for light microscopy observations were cut with the help of Accutem -50 produced by Struers and mounted into an acrylic cold mounting resin ClaroCit from Struers. In order to ensure the flat and smooth specimen surface, the specimens were grinded and polished with the Tegramin-25 preparation system. Thereafter, specimens were electrolytically etched with the Barker's method on the LectroPol-5 apparatus. The specimens were etched at 25 V for 180 s at 8 ˚C with a flow rate of 10 ml/s using the Barker solution (12 ml HBF_4 (35%) + 400 ml H_2O), their microstructure was studied with the optical microscope Olympus IX70 produced by OLYMPUS.

2.2.3. Deformation tests

Specimens for compression tests with a gauge of (23.5x11.5x12) mm^3 were machined from a round bar of 6082 alloy with a diameter of 60 mm by Accutom-50 from Struers. The deformation axis was parallel to extrusion direction (ED). Before the measurement, specimens were heat treated and quenched into water.

The dog bone shaped specimens for tensile tests with a gauge of (120x20.5x1.15) mm^3 and with a deformation axis oriented parallel to the rolling direction were prepared from a cold rolled 5182 sheet. The specimens, before the measurements, were heat treated and quenched into water.

The parameters of the heat treatment are presented in Table 3. The uniaxial deformation tests were performed using a universal testing machine Instron 5882 at room temperature (RT), with constant cross-head speeds giving the strain rates of $\dot{\varepsilon}$ = (10^{-4} and 10^{-3})s^{-1} (see Table 4). Specimens were deformed in case of compression tests up to 80 kN, in case of tensile tests up to fracture. The sampling frequency was 20 Hz. The evaluation process was done by Bluehill® software from Instron©.

2.2.4. Acoustic emission measurements

The measurement and analysis of the AE data was performed by a computer controlled diagnostic system DAKEL-IPL-4, developed by company ZD RPETY-DAKEL. A piezoelectric sensor MICRO 2006 with a diameter of 3.4 mm and a flat response in a frequency range of (100-600) kHz was used. The sensor was attached to the specimen's surface with the help of a clip and silicon grease which improves the contact between the specimen and AE sensor. To keep a high ratio between AE signal and a noise, a preamplifier of 35 dB was used.

DAKEL-IPL-4 system enables a continuous storage of AE signal on 4 channels with a different amplification (0, 10, 20 and 30 dB – in this work) which allows the elimination of the omissions/overflows of recoded data. A 12-bit A/D converter with a sampling frequency of 2 MHz having full scale of ± 2 V was used. The DAKEL-IPL-4 was connected with the computer via a network cable. The measured AE data were stored on an external disc with a bite rate of 16 MB/s and later analysed by the DAKEL-UI software from ZD RPETY-DAKEL.

By the evaluation of the AE events from the data stream, the threshold for the AE event was pre-set to 0.01 mV and the separation time of two events (the minimum time between the end of the last and the beginning of the next AE event) was set to 0.30 ms. The minimal and the maximal hit length was set to 0.05 and 1000 ms, respectively. The dead time was $t_d = 7.10^{-4}$s. By the evaluation of the AE counts, the thresholds were set to 15% and 30% of the whole range.

The obtained data were evaluated with Origin® software produced by OriginLab®.

3. Results

3.1. Microstructure

Specimen	*Temperature [˚C]*	*Duration [h]*	*Deformation speed [s^{-1}]*
D$10^{-3}s^{-1}$	-	-	10^{-3}
D$10^{-4}s^{-1}$	-	-	10^{-4}
D$10^{-3}s^{-1}$1h530˚C	530	1	10^{-3}
D$10^{-4}s^{-1}$1h530˚C	530	1	10^{-4}
D$10^{-3}s^{-1}$4h530˚C	530	4	10^{-3}
D$10^{-4}s^{-1}$4h530˚C	530	4	10^{-4}
T$10^{-3}s^{-1}$2h400ºC	400	2	10^{-3}

Table 4. Parameters of the heat treatment and deformation tests for investigated specimens (D - deformed in compression, T - deformed in tension)

The microstructure of selected specimens before and after electro-etching can be seen in Figs. 3-5.

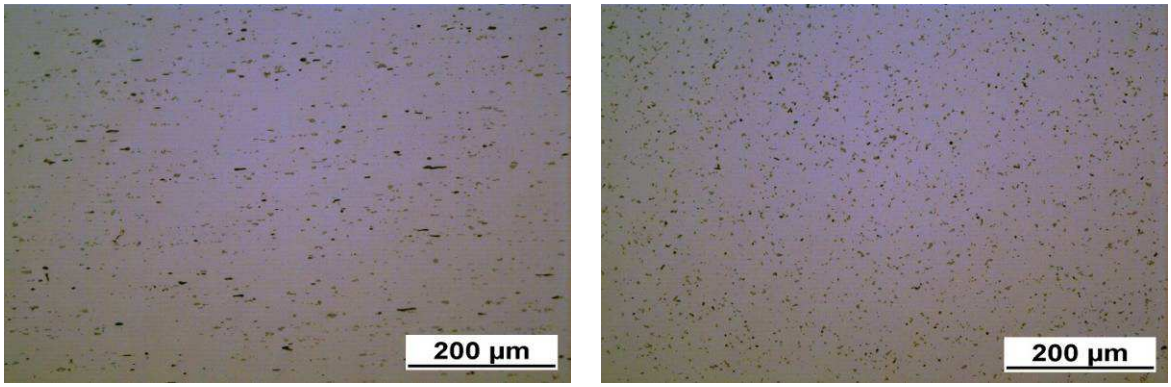

a) b)

Fig. 3: Microstructure of 6082 alloy in as-received condition; sample's surface is a) parallel b) perpendicular to extrusion direction

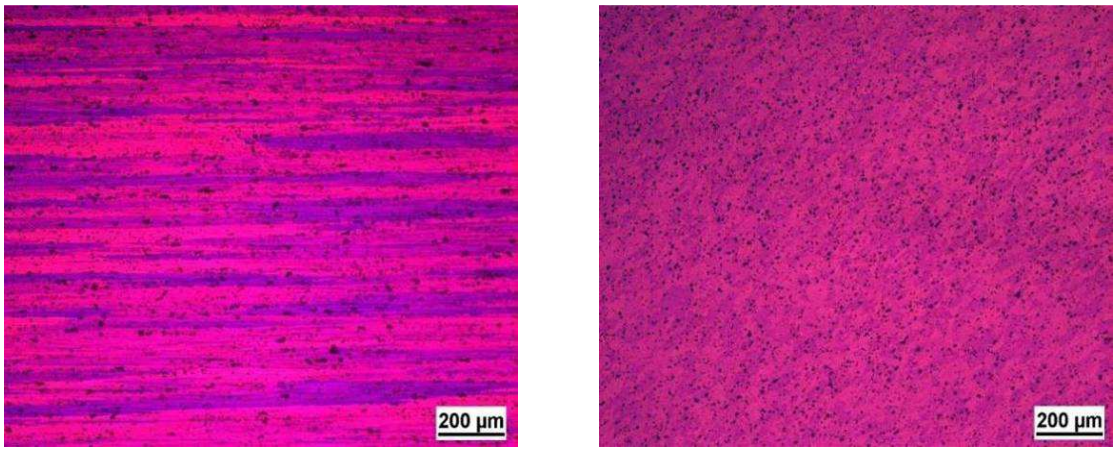

a) b)

Fig. 4: Microstructure of 6082 alloy in as-received condition after etching; specimen's surface is a) parallel b) perpendicular to extrusion direction

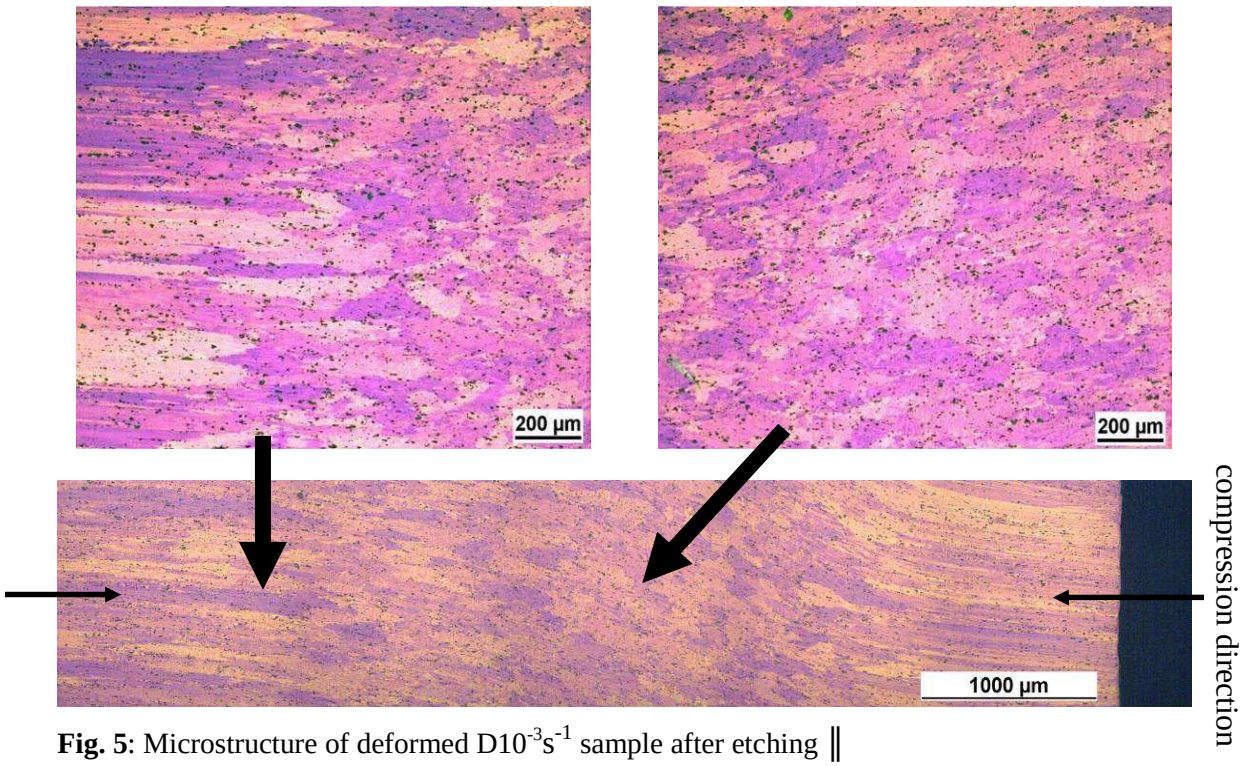

Fig. 5: Microstructure of deformed $D10^{-3}s^{-1}$ sample after etching ‖

The microstructure of 6082 alloy in as-received condition (non-heat treated) is shown in Fig. 3. Distribution of particles on specimen's surface, which was taken parallel to ED , is inhomogeneous with a spread of particles into ED (Fig. 3a) and on transversal specimen's surface to ED is homogeneous (Fig. 3b). The microstructure consists of grains elongated into ED (Fig. 4).

Fig. 5 shows the microstructure of deformed $D10^{-3}s^{-1}\parallel$ sample after etching. It can be seen a bimodal microstructure with almost equiaxial grains in the middle part and elongated grains at the edge of the specimen.

The average microhardness of the non-deformed (N) and deformed (D) specimens can be seen in Table 5.

Specimen	*HV0.1*	σ_{HV}
N$\parallel$	100.18	2.50
N$\perp$	101.29	1.86
$D10^{-3}s^{-1}\parallel$	134.63	3.44
$D10^{-3}s^{-1}\perp$	137.44	3.28
$D10^{-3}s^{-1}$4h530˚C$\parallel$	121.49	3.38
$D10^{-3}s^{-1}$4h530˚C $\perp$	118.99	3.49
N1h530˚C $\parallel$	95.59	1.87
N1h530˚C $\perp$	95.11	1.57
N4h530˚C $\parallel$	94.90	1.56
N4h530˚C $\perp$	95.98	1.86

Table 5. The average microhardness of specimens and its standard deviation (σ_{HV})

Microhardness of the specimens in the as-received condition (non-heat treated) is higher than for the heat treated specimens. No significant difference in microhardness values between parallel and perpendicular direction to ED was determined. Furthermore, with increasing annealing time no changes in microhardness were observed.

The maps of the microhardness of selected specimens are presented in Figs. 6-10. It is clearly seen that the microhardness of the specimens is almost homogenous and only the deformed specimens show some areas with a slightly higher or lower microhardness.

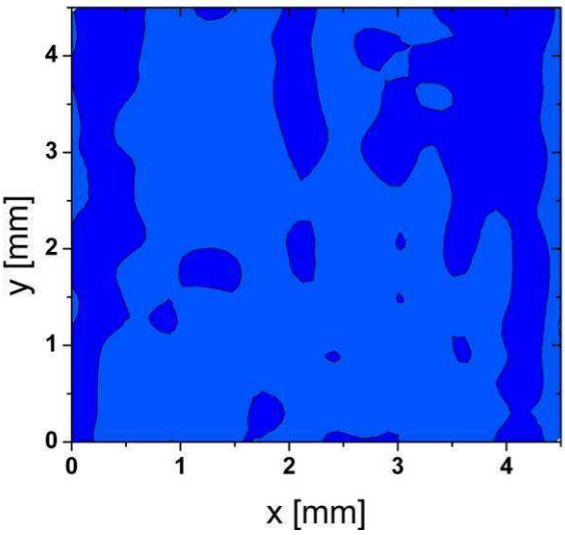

Fig. 6: The microhardness map of the N1h530˚C specimen parallel to ED (N1h530˚C‖)

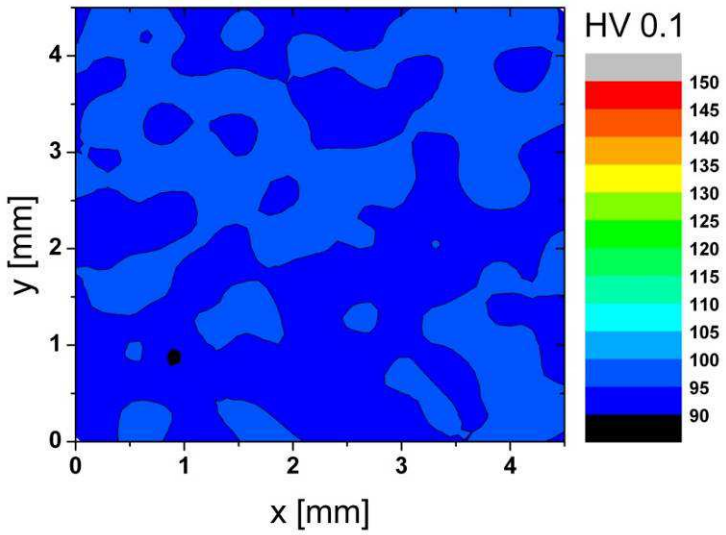

Fig. 7: The microhardness map of the N4h530˚C specimen parallel to ED (N4h530˚C‖)

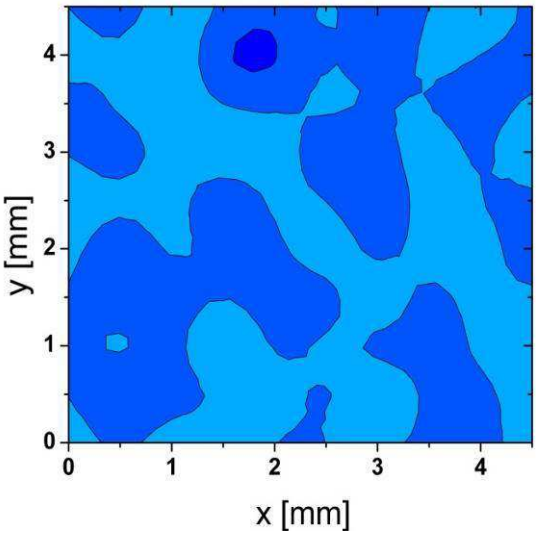

Fig. 8: The microhardness map of the non-deformed specimen parallel to ED (N‖)

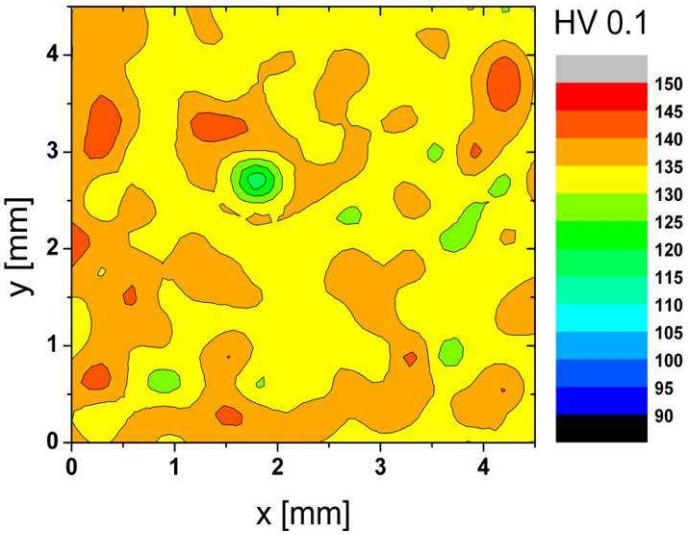

Fig. 9: The microhardness map of the $D10^{-3}s^{-1}$ specimen parallel to ED ($D10^{-3}s^{-1}$‖)

Fig. 10: The microhardness map of the $D10^{-3}s^{-1}4h530^{\circ}C$ specimen parallel to ED ($D10^{-3}s^{-1}4h530^{\circ}C \parallel$)

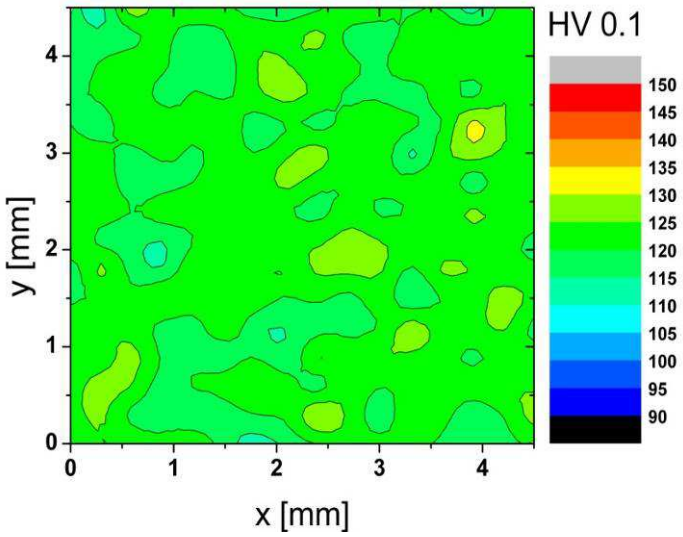

3.4. Deformation tests and acoustic emission measurements

Compressive stress-time curves with concurrent AE measurements are plotted in Figs. 11-28. For each deformation curve two details, taken from a low and a high strain region, are presented. Details have a uniform scale of $\Delta\sigma$ = 8 MPa.

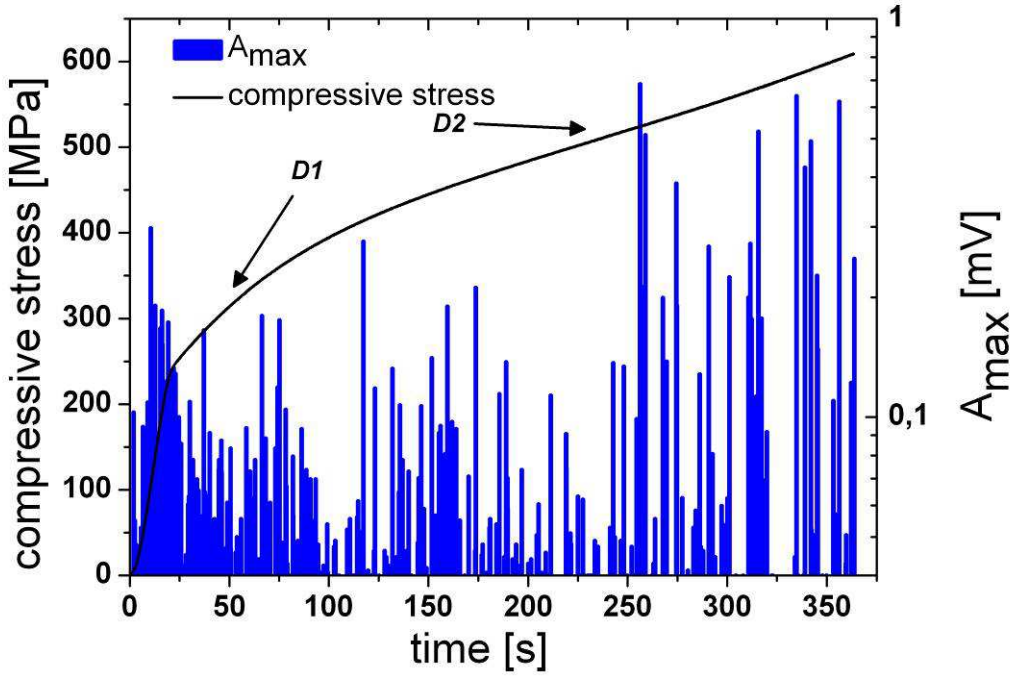

Fig. 11: The stress-time curve for the D10 $^{-3}$s^{-1} specimen correlated with the A_{max}

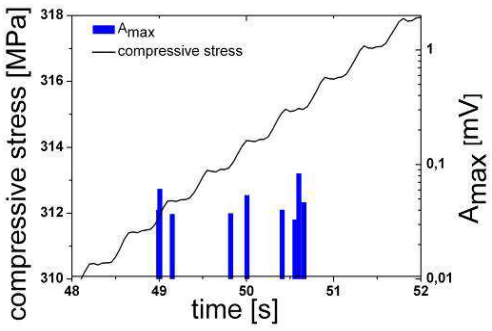

Fig. 12: Detail D1 from Fig. 11

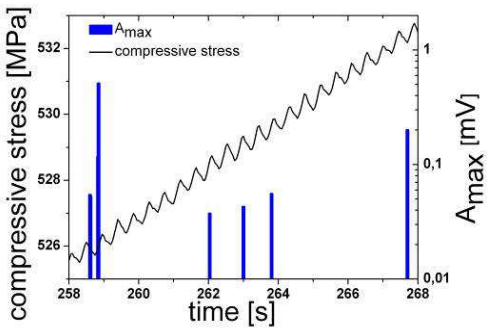

Fig. 13: Detail D2 from Fig. 11

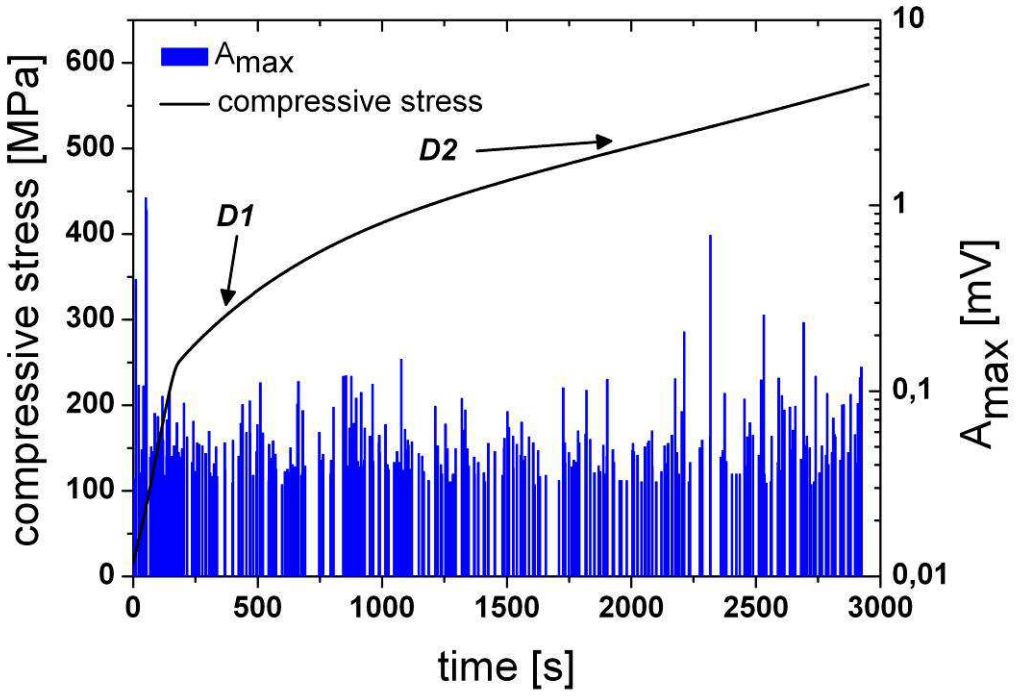

Fig. 14: The stress-time curve for the D10 $^{-4}$s^{-1} specimen correlated with the A_{max}

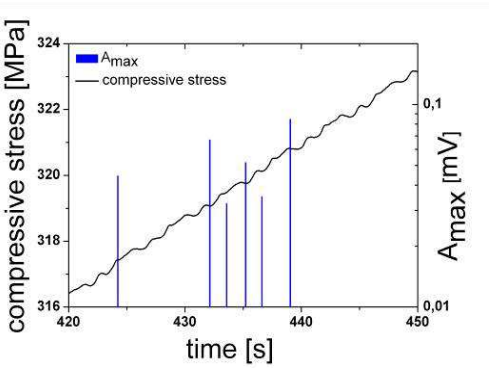

Fig. 15: Detail D1 from Fig. 14

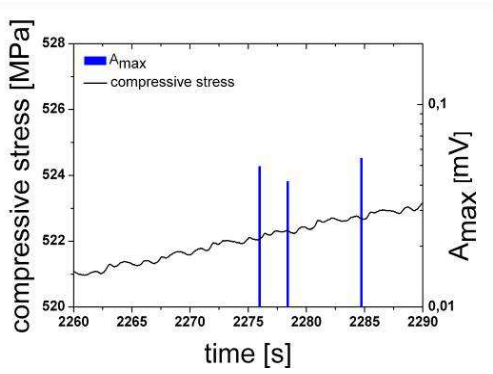

Fig. 16: Detail D2 from Fig. 14

The deformation curves correlated with the maximum amplitude (A_{max}) of the AE events for the non-heat treated specimens can be seen in Figs. 11-16. Fig. 12 shows a detail of low strain region for D10 $^{-3}$s^{-1} specimen, where the deformation curve is regularly serrated with relatively small amplitude. In the high strain region (Fig. 13), the serration consists of stress increments and drops with slightly smaller amplitude than for the low strain region. The specimen, which was deformed with a smaller strain rate (D10 $^{-4}$s^{-1}), exhibits at small strains a more irregular serration comparing to D10 $^{-3}$s^{-1} specimen which can be seen in Fig. 15. At high strains, for both D10 $^{-3}$s^{-1} and D10 $^{-4}$s^{-1} specimens (Figs. 13 and 16) a similar behaviour was observed.

Figs. 17-28 show deformation curves correlated with the A_{max} for heat treated specimens deformed in compression. Different forms of serration on the deformation curve in comparison to non-heat treated specimens were observed. For all heat treated specimens, in the low strain region (Figs. 18, 21, 24, 27), there is a coexistence of large stress jumps with small serrations on deformation curve. In high strain region (Figs. 19, 22, 25, 28), only small serrations on deformation curve were observed.

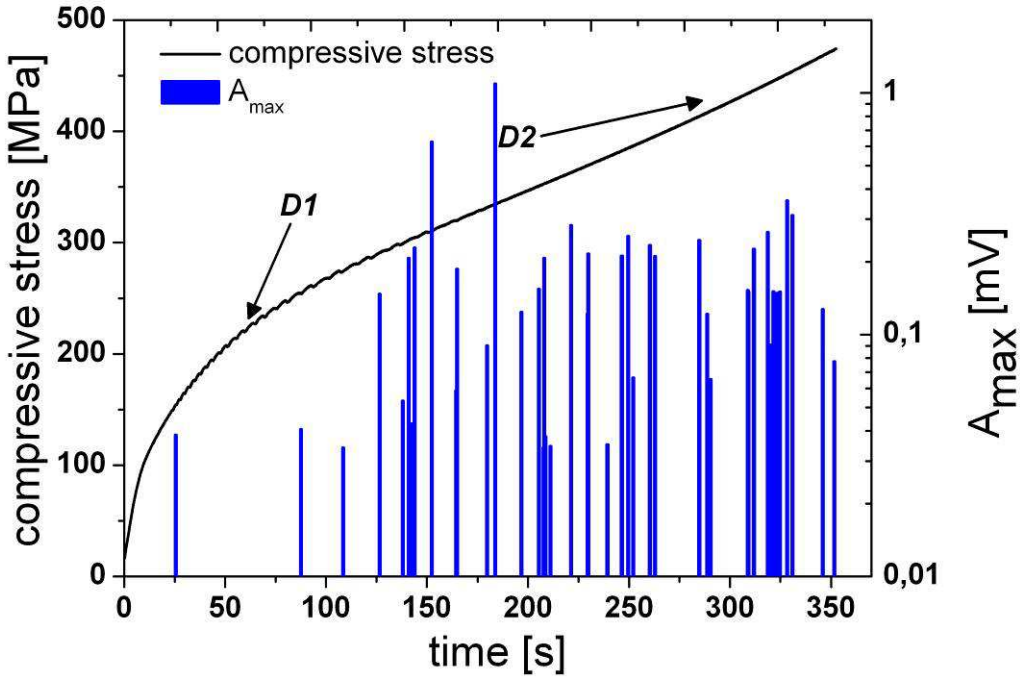

Fig. 17: The stress-time curve for the D10 $^{-3}$ s^{-1}1h530˚C specimen correlated with the A_{max}

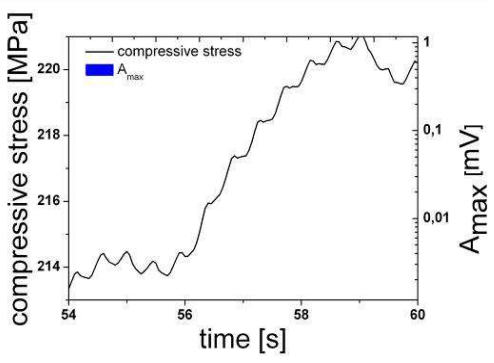

Fig. 18: Detail D1 from Fig. 17

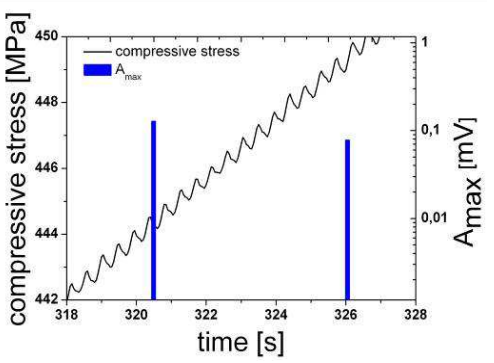

Fig. 19: Detail D2 from Fig. 17

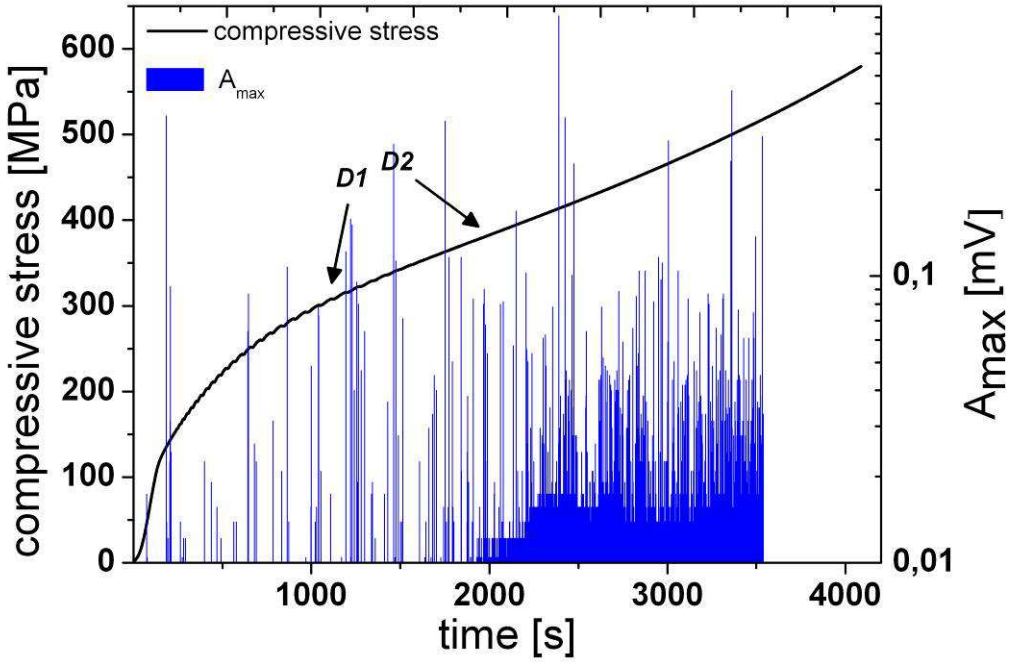

Fig. 20: The stress-time curve for the D10 $^{-4}$s^{-1}1h530˚C specimen correlated with the A_{max}

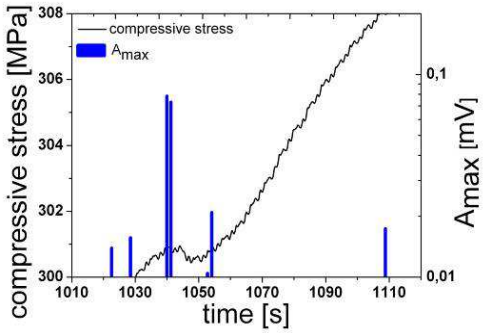

Fig. 21: Detail D1 from Fig. 20

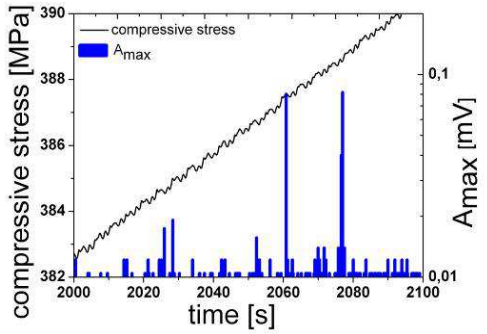

Fig. 22: Detail D2 from Fig. 20

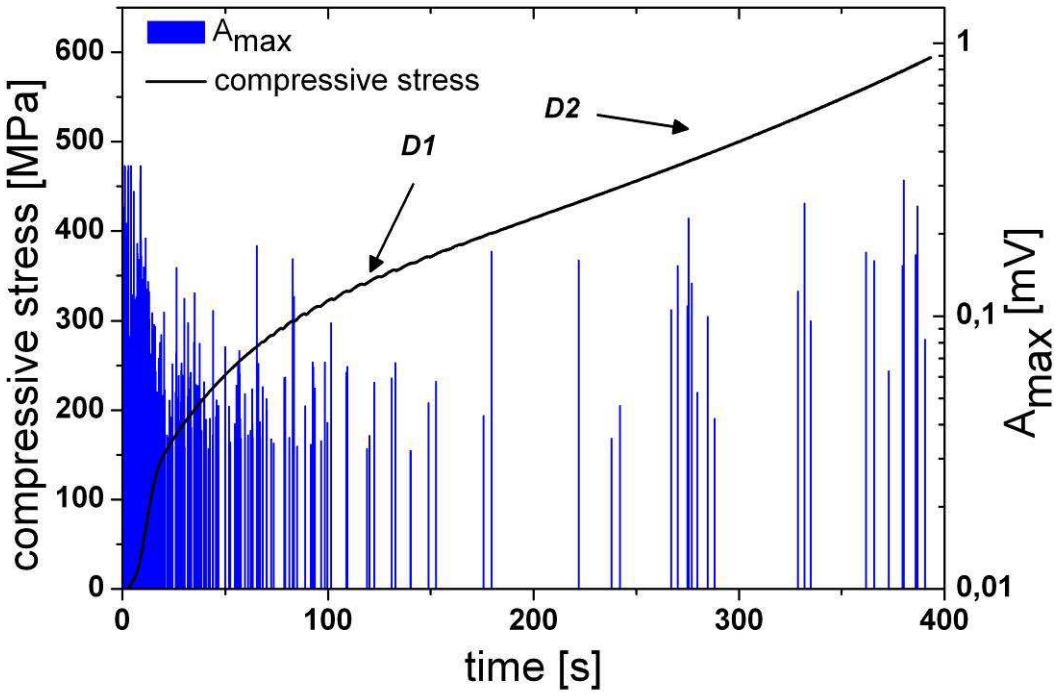

Fig. 23: The stress-time curve for the D10 $^{-3}$ s^{-1} 4h530˚C specimen correlated with the A_{max}

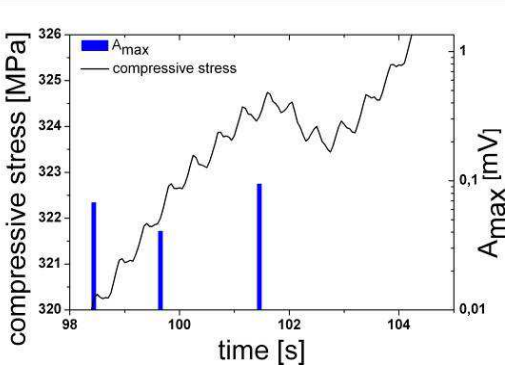

Fig. 24: Detail D1 from Fig. 23

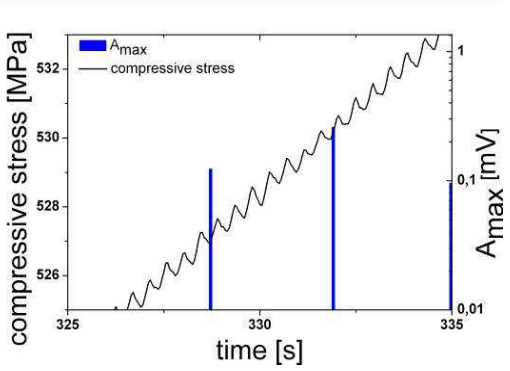

Fig. 25: Detail D2 from Fig. 23

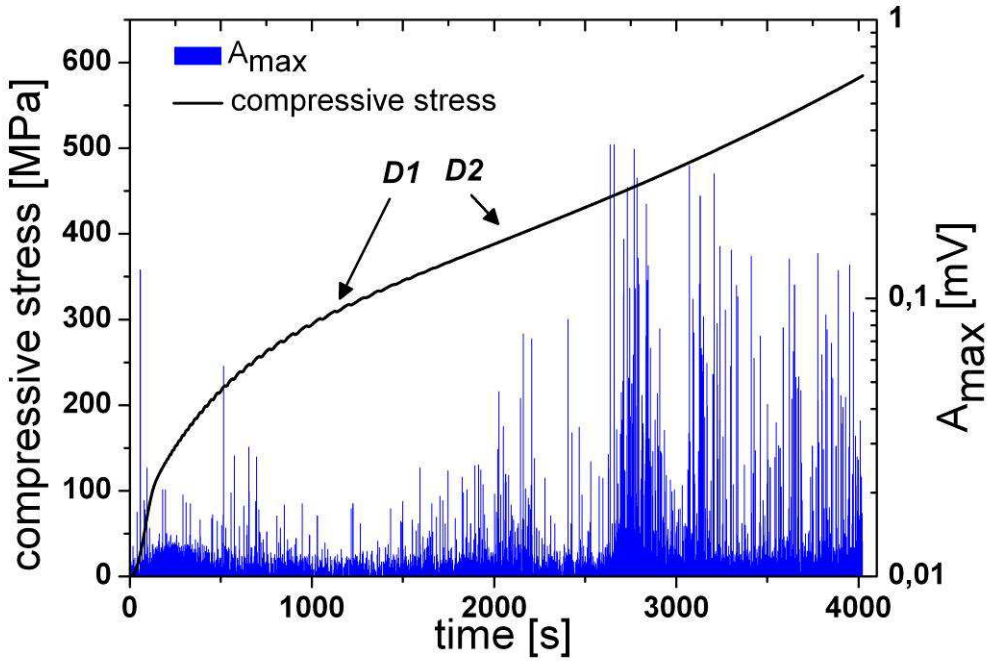

Fig. 26: The stress-time curve for the D10^{-4}s^{-1}4h530˚C specimen correlated with the A_{max}

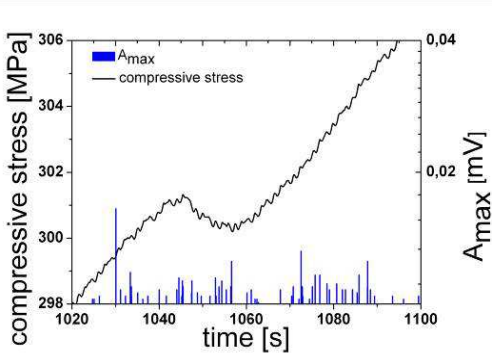

Fig. 27: Detail D1 from Fig. 26

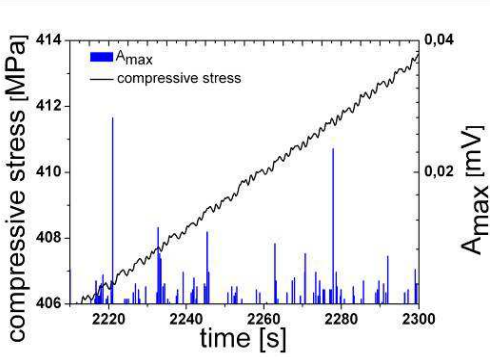

Fig. 28: Detail D2 from Fig. 26

Comparing the results obtained from D10^{-3}s^{-1} 1h530˚C and D10^{-3}s^{-1}4h530˚C, it can be seen that serrations are similar (Figs. 18, 19 and 24,25). The serrations have a regular frequency and amplitude.

The heat treated specimens deformed at a lower strain rate D10^{-4}s^{-1} 1h530˚C and D10^{-4}s^{-1}4h530˚C (Figs. 21, 22 and 27,28) also show similar serrations on deformation curve. The serration has a very irregular frequency and amplitude.

More AE events (higher number of A_{max} data) were observed in heat treated than in non-heat treated specimens. In the case of the specimens deformed at a higher strain rate (specimens D10^{-3}s^{-1}, D10^{-3}s^{-1} 1h530˚C and D10^{-3}s^{-1}4h530˚C), some areas where no AE events (represented by A_{max}) can be seen (Figs. 11, 17 and 23).

The specimens deformed at lower strain rate (specimens D10^{-4}s^{-1}, D10^{-4}s^{-1} 1h530˚C and D10^{-4} s^{-1}4h530˚C) usually exhibit some value of A_{max} during whole test (Figs. 14, 20 and 26). For all specimens, the value of the A_{max} was under 1mV. It is noteworthy that the A_{max} does not accurately correlate with the large serrations on the deformation curves.

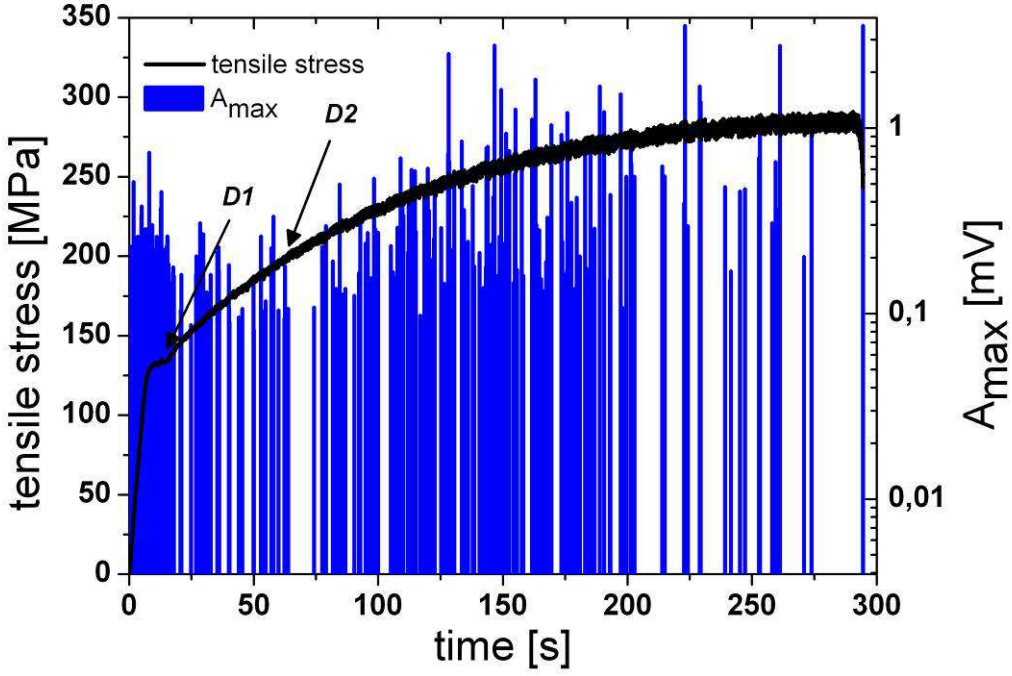

Fig. 29: The stress-time curve for the T10^{-3}s^{-1}2h400ºC specimen correlated with the A_{max}

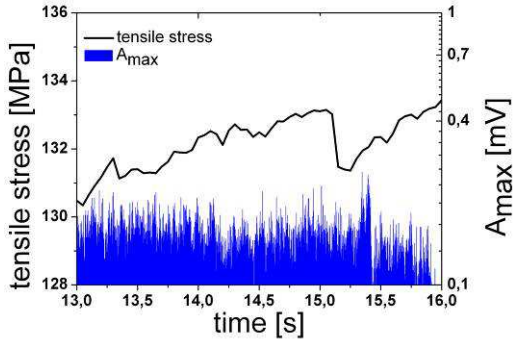

Fig. 30: Detail D1 from Fig. 29

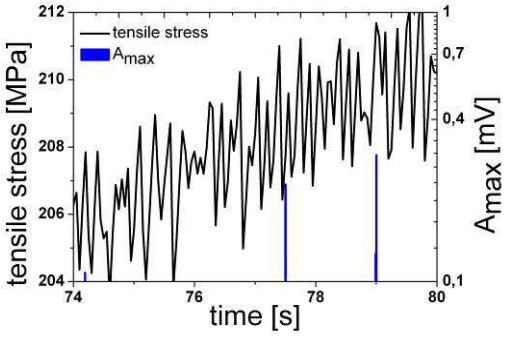

Fig. 31: Detail D2 from Fig. 29

The correlation of A_{max} with the tensile curve for the T10^{-3}s^{-1}2h400ºC specimen can be seen in Fig. 29. At the beginning of the deformation, where a deformation plateau occurs, a remarkable AE response was observed. Thereafter AE

intensity decreases and high values of A_{max} were detected in the middle and at the end of the experiment.

Fig. 30 shows a detail of low strain region for the T10^{-3}s^{-1}2h400ºC specimen. In this area, a high AE activity with relatively low A_{max} was detected. The corresponding tensile curve shows irregular stress jumps with a much lower frequency than the frequency of this area's AE events. Detail of high strain region for the T10^{-3}s^{-1}2h400ºC specimen (Fig. 31) shows large irregular serrations almost without AE events.

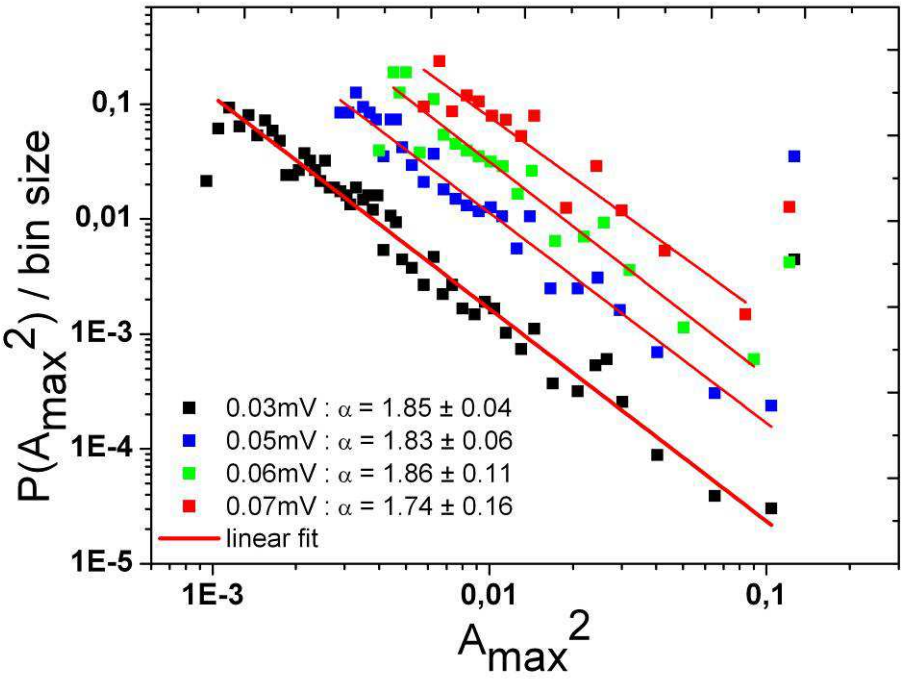

Fig. 32: Effect of the threshold voltage set up on the probability density of squared maximal amplitudes of AE events for the D10^{-3}s^{-1}4h530ºC specimen

The effect of the threshold voltage set up, used for the determination of the AE events from data streaming, on the probability density of squared maximal amplitudes of AE events for the D10^{-3}s^{-1}4h530ºC specimen can be seen in Fig. 32. It is obvious that the exponent of power law distribution is independent of the choice of the threshold voltage. The exponent values obtained for different threshold voltages are equal in frame of errors.

Figs. 32-39 show the probability density function of the squared maximal amplitude for selected specimens. It is clearly seen that all data show a linear trend.

The values of the exponent α from power law distribution for specimens are presented in Table 6.

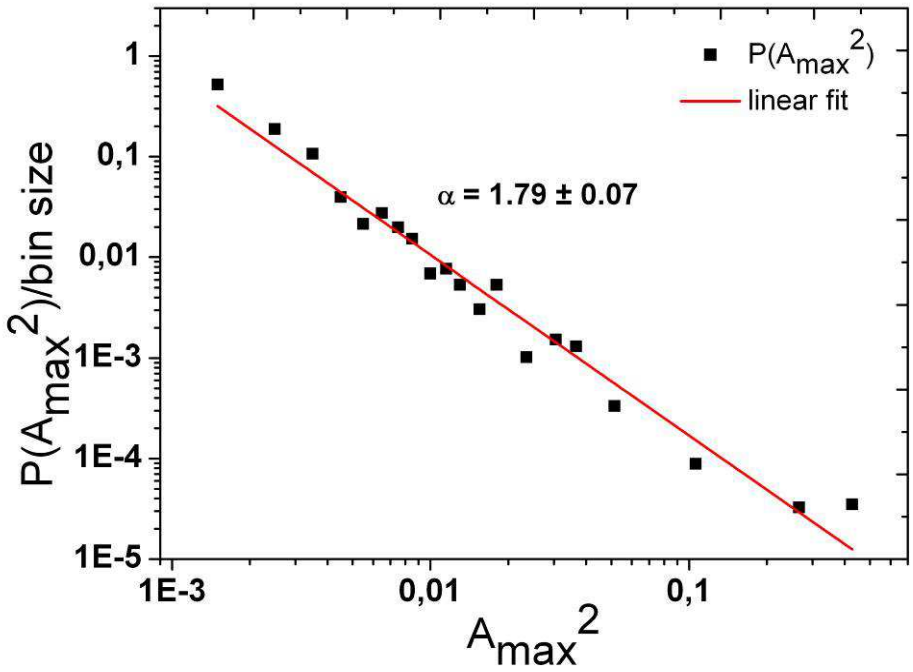

Fig. 33: The probability density function of the squared maximal amplitude for the D10^{-3}s^{-1} specimen

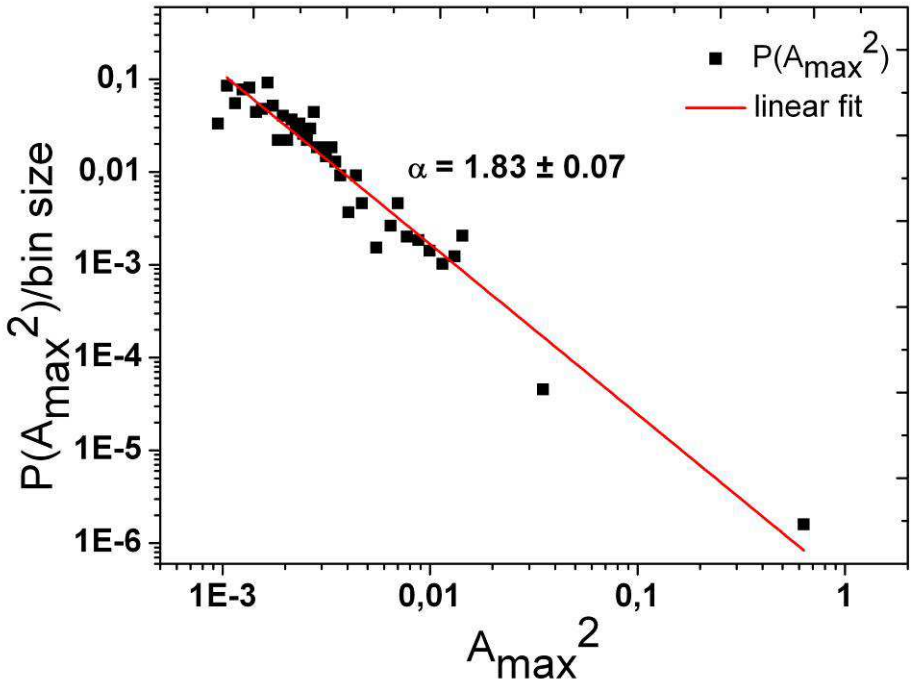

Fig. 34: The probability density function of the squared maximal amplitude for the D10^{-4}s^{-1} specimen

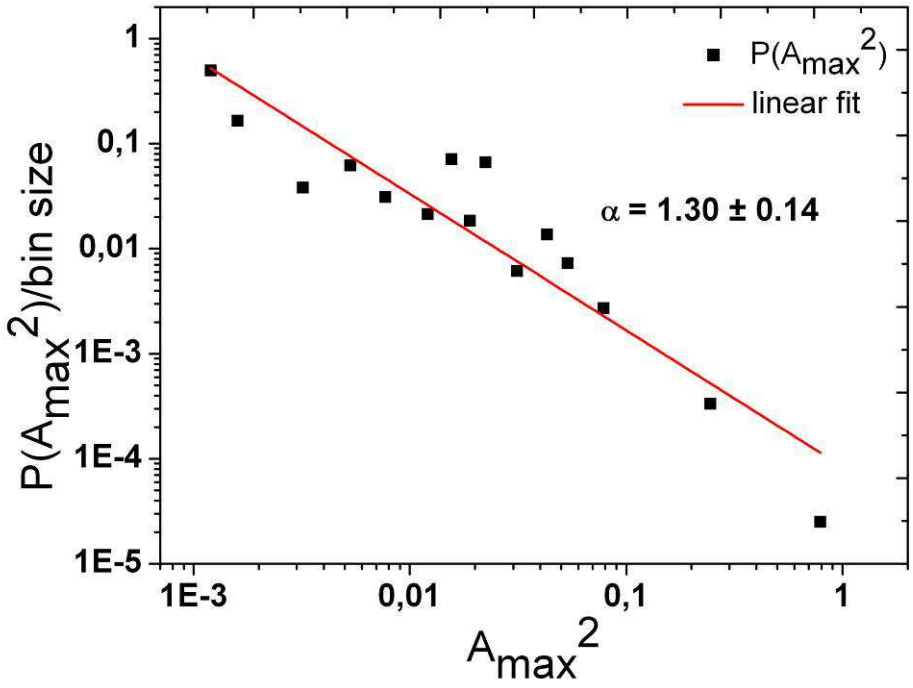

Fig. 35: The probability density function of the squared maximal amplitude for the D10^{-3}s^{-1}1h530ºC specimen

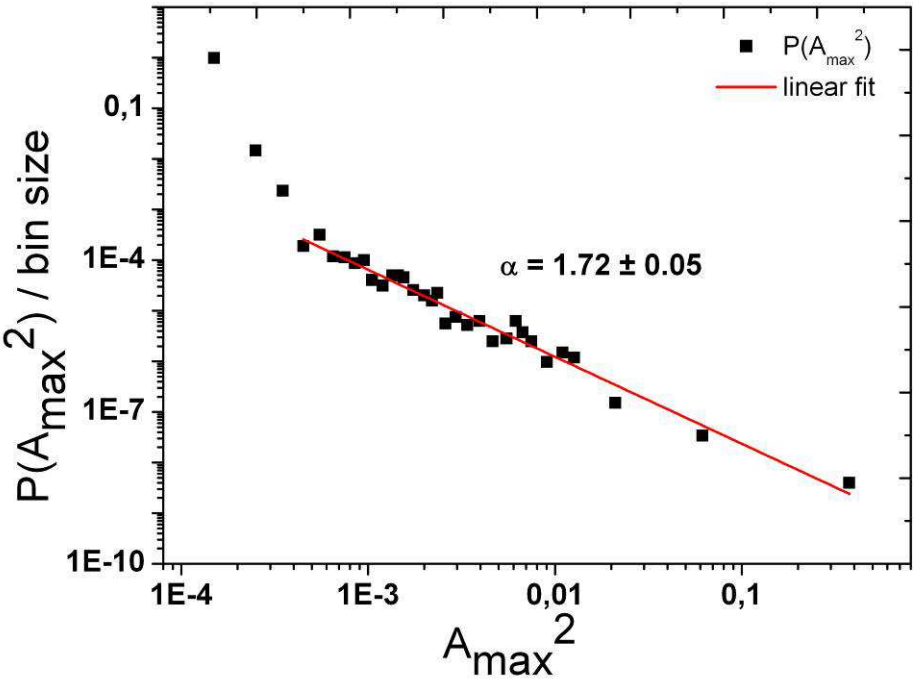

Fig. 36: The probability density function of the squared maximal amplitude for the D10^{-4}s^{-1}1h530ºC specimen

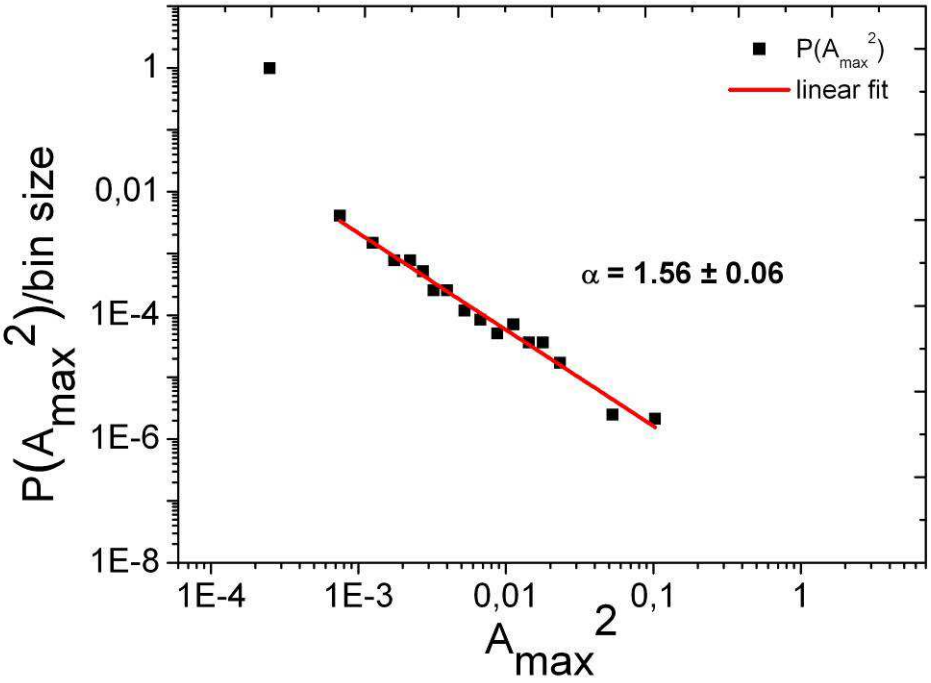

Fig. 37: The probability density function of the squared maximal amplitude for the D$10^{-4}s^{-1}$4h530ºC specimen

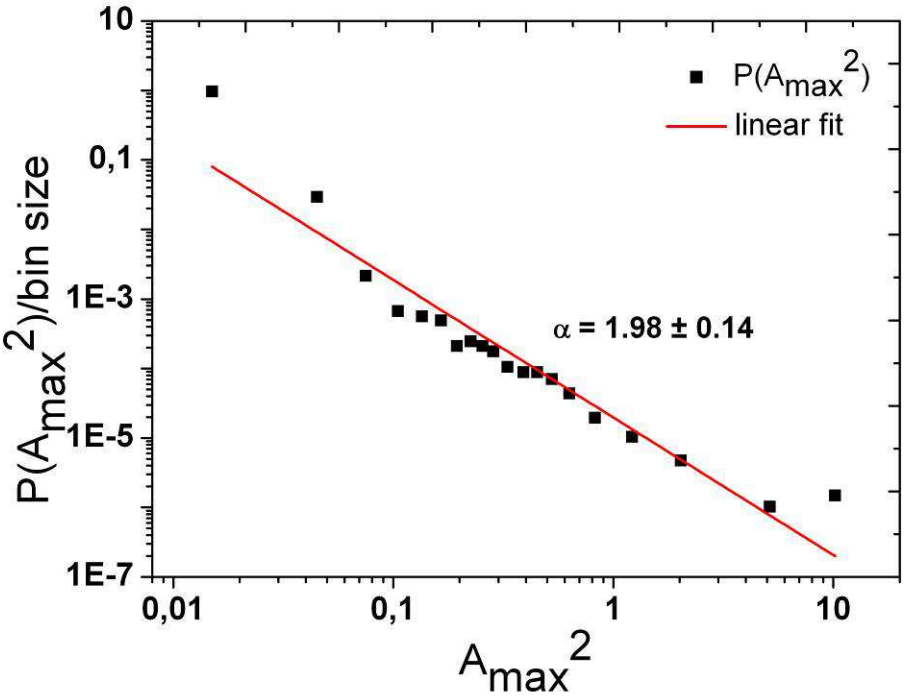

Fig. 38: The probability density function of the squared maximal amplitude for the T$10^{-3}s^{-1}$2h400ºC specimen

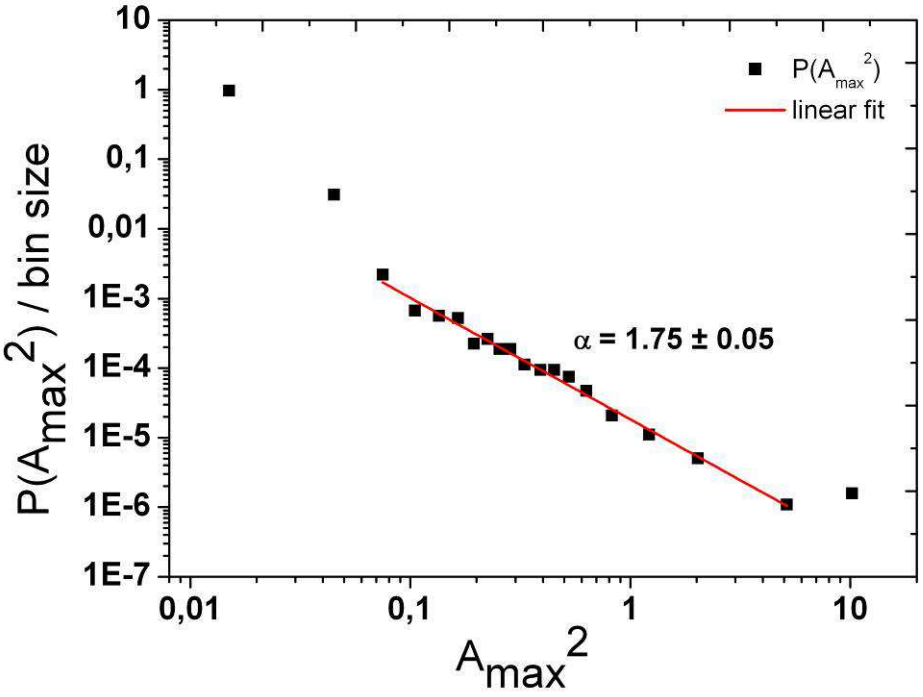

Fig. 39: The probability density function of the squared maximal amplitude for the T10^{-3}s^{-1}2h400ºC specimen from the region of the PLC phenomenon

Almost in all cases, some points, occurring at the beginning (Fig. 39) or at the end of the data set (Fig. 33), are out of the linear dependence.

Specimen	α	σ_α
D10^{-3}s^{-1}	1.79	0.07
D10^{-4}s^{-1}	1.83	0.07
D10^{-3}s^{-1}1h530ºC	1.30	0.14
D10^{-4}s^{-1}1h530ºC	1.72	0.05
D10^{-3}s^{-1}4h530ºC	1.84	0.07
D10^{-4}s^{-1}4h530ºC	1.56	0.06
T10^{-3}s^{-1}2h400ºC	1.98	0.14
T10^{-3}s^{-1}2h400ºC - PLC phenomenon	1.75	0.05

Table 6: Exponent α of the linear fits for the probability density function of the squared maximal amplitude and its standard deviation (σ_α)

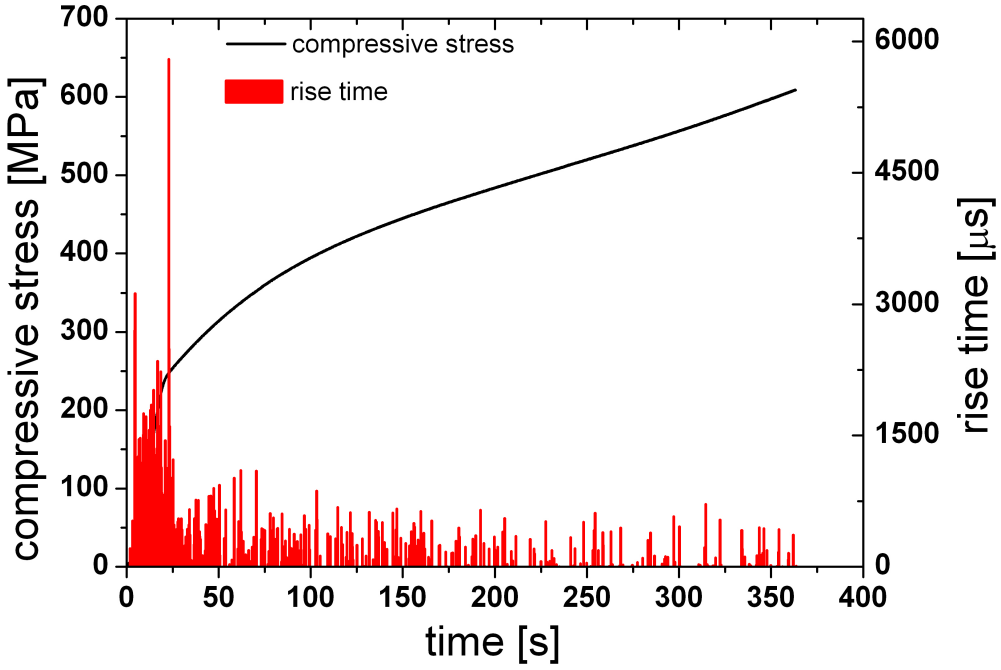

Fig. 40: The rise time of the AE events correlated with the deformation curve for the $D10^{-3}s^{-1}$ specimen

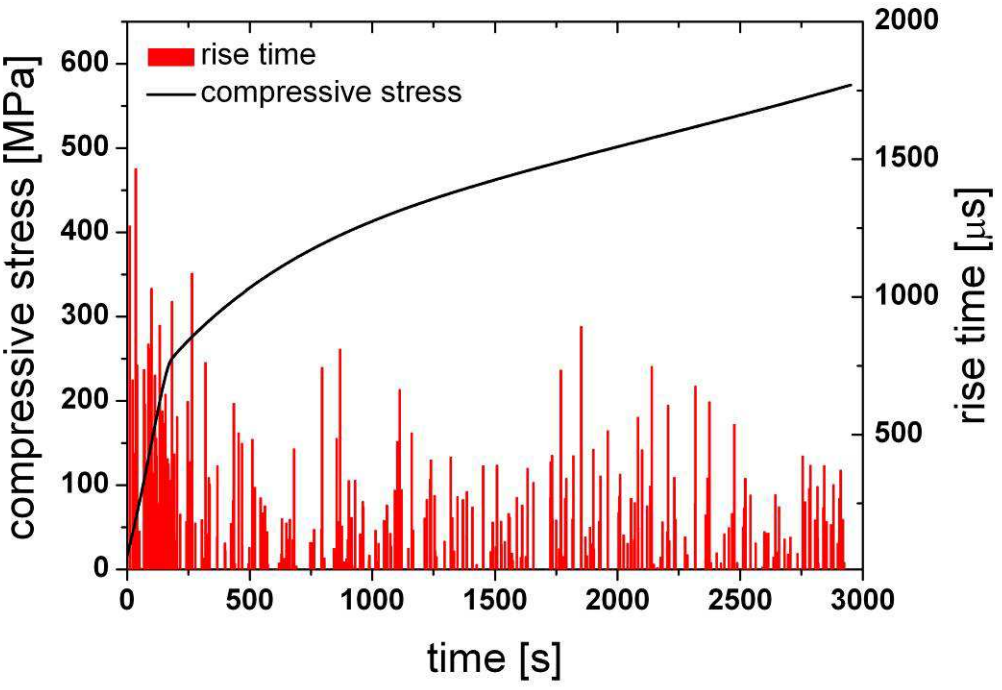

Fig. 41: The rise time of the AE events correlated with the deformation curve for the $D10^{-4}s^{-1}$ specimen

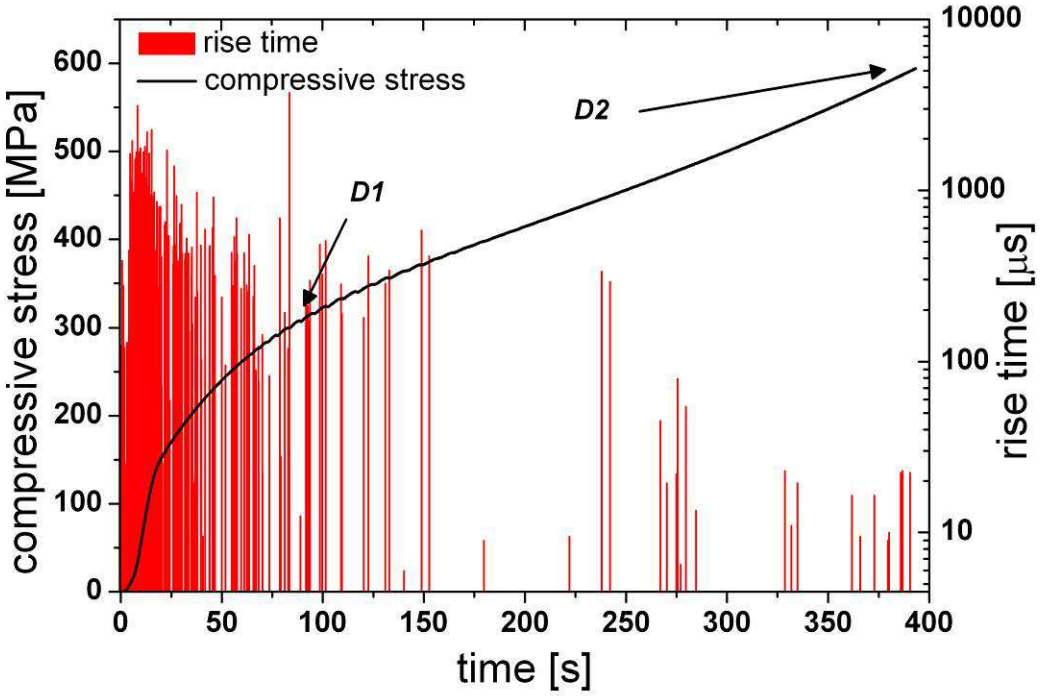

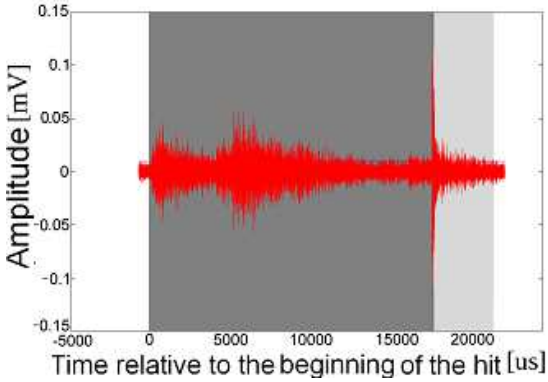

D1) the first AE event for Fig. 42

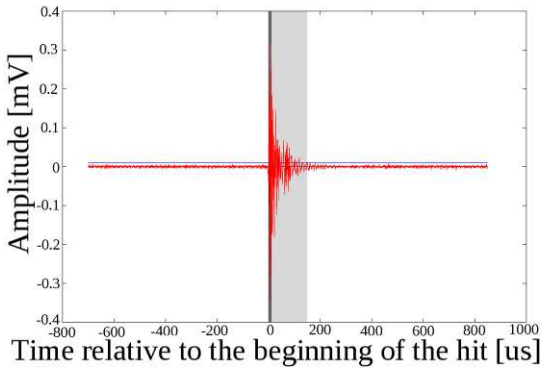

D2) the second AE event for Fig. 42

Fig. 42: The rise time of the AE events correlated with the deformation curve for the D$10^{-3}s^{-1}$4h530ºC specimen and examples of AE events determined from the denoted area

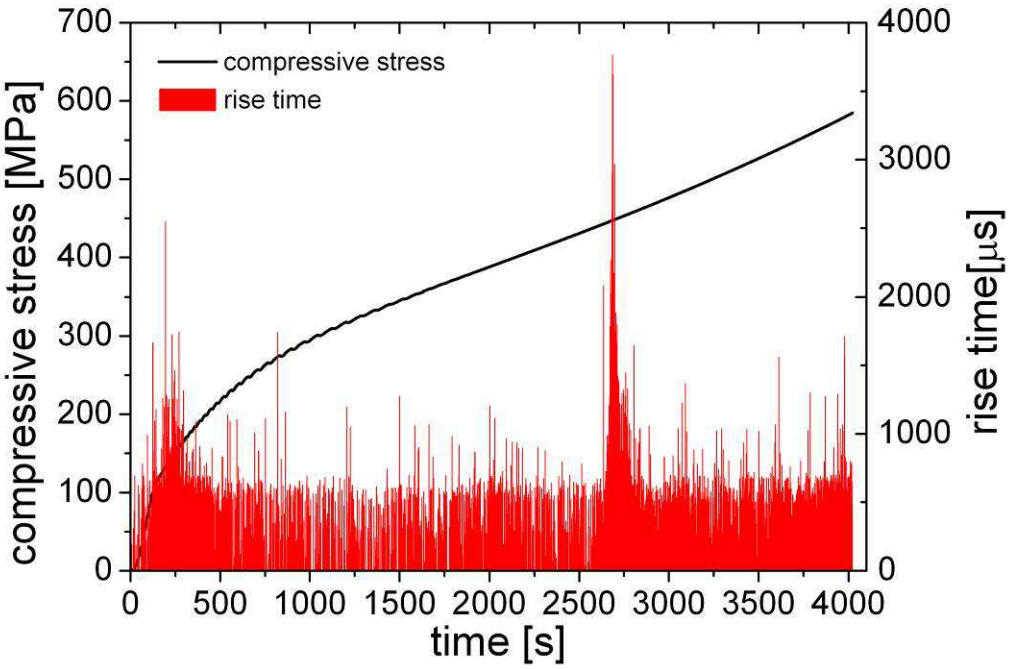

Fig. 43: The rise time of the AE events correlated with the deformation curve for the D10^{-4}s^{-1}4h530ºC specimen

For all specimens, high rise time is observed at the beginning of plastic deformation. Figs. 40 and 41 of non-heat treated D10^{-3}s^{-1} and D10^{-4}s^{-1} specimens show that the average rise time of the AE events was about 1000 μs. It can also be seen that before an AE event with a high rise time more AE events with a shorter rise time occur. Figures 42 and 43, for the heat treated specimens (D10^{-3}s^{-1}4h530ºC, D10^{-4}s^{-1}4h530ºC), show that the rise time for the large stress jumps is lower (about 100-1000 μs) than it was for the non-heat treated specimens.

In the case of the heat treated D10^{-3}s^{-1}4h530ºC specimen (Fig. 42), high values of rise time are observed at the beginning of deformation and a maximum (almost 4000 μs) was found with a progress of plastic deformation.

The figures D1, D2 at Fig. 42 shows AE events determined from the continuous AE data streaming with the help of Dakel UI software. The duration of the AE event is designated by gray and the rise time by dark gray colour. The first detail D1 shows that the determined AE event consists of more small AE events. Events with smaller A_{max} are included into the rise time area of the evaluated AE

event. The D2 detail shows a signal with a short rise time and high A_{max} detected at the end of the compression test.

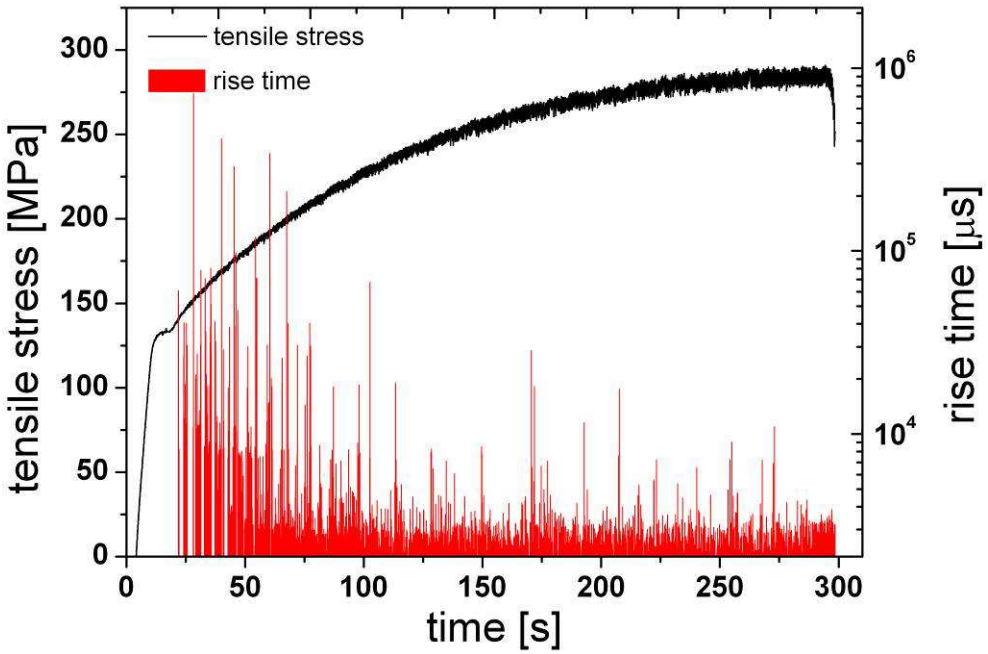

Fig. 44: The rise time of the AE events correlated with the deformation curve for the specimen 5182 deformed in tension T10^{-3}s^{-1}2h400ºC

The rise time of the AE events correlated with the deformation curve for the 5182 specimen deformed in tension T10^{-3}s^{-1}2h400ºC can be seen in Fig. 44. In the area of the strain hardening, rise time maxima with a magnitude of 0,1 s were observed. Also in this case before these rise time maxima there are other smaller rise time values, which stepwise increase till these maxima. In the following area it can be seen that the PLC phenomenon has a low rise time with a magnitude of 10^3 μs.

The dependence of the A_{max} on the rise time of the AE event can be seen in Figs. 45-49.

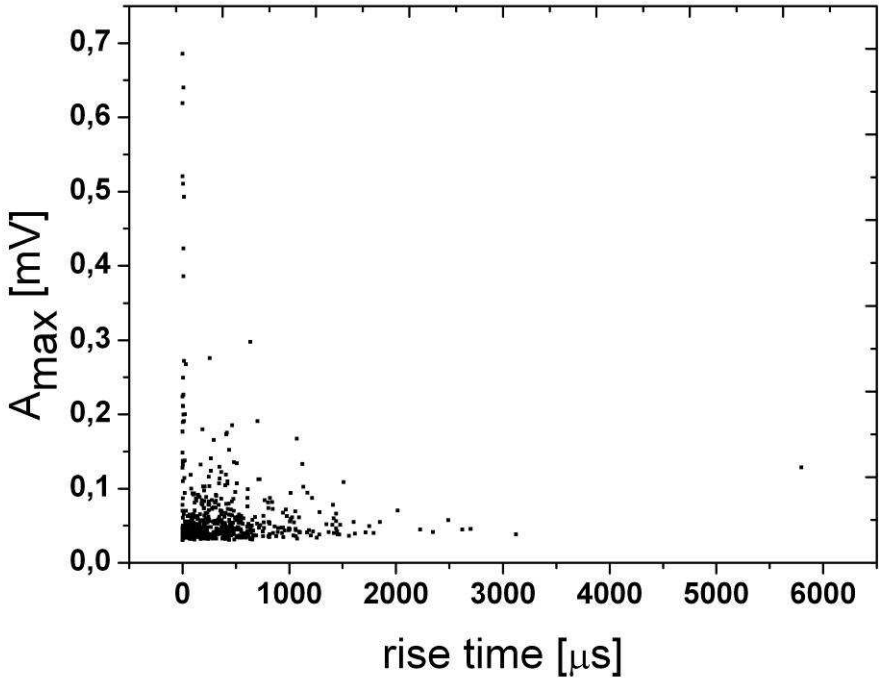

Fig. 45: The dependence of the A_{max} on the rise time of the AE events for the $D10^{-3}s^{-1}$ specimen

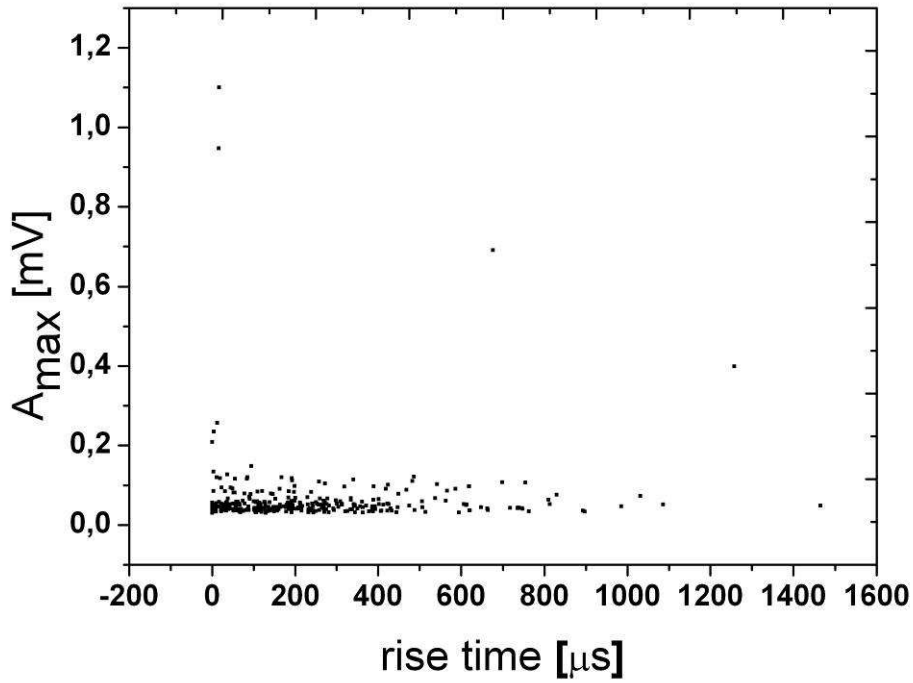

Fig. 46: The dependence of the A_{max} on the rise time of the AE events correlated with the deformation curve for the $D10^{-4}s^{-1}$ specimen

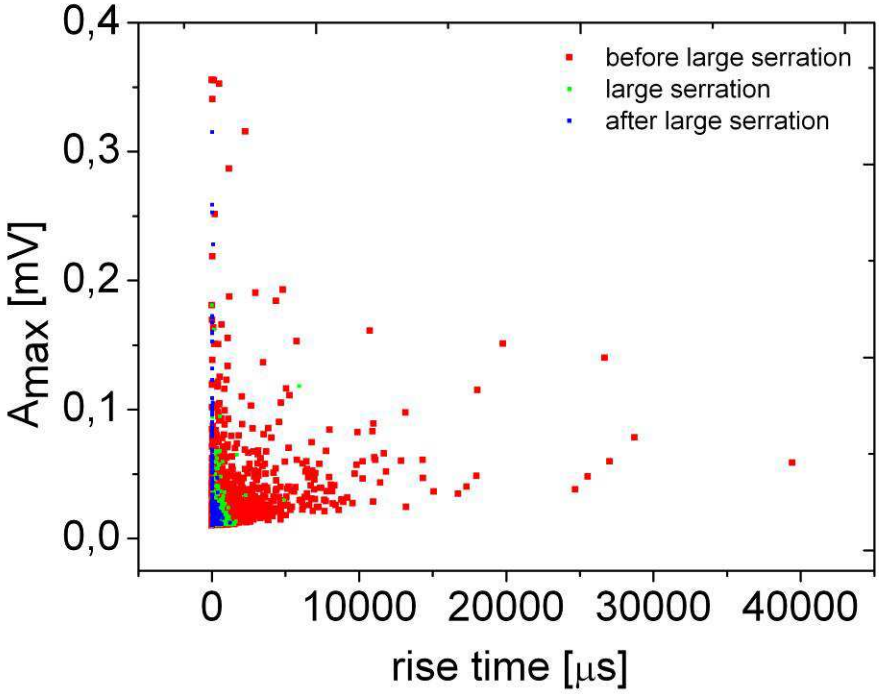

Fig. 47: The dependence of the A_{max} on the rise time of the AE events correlated with the deformation curve for the D10^{-3}s^{-1}4h530ºC specimen

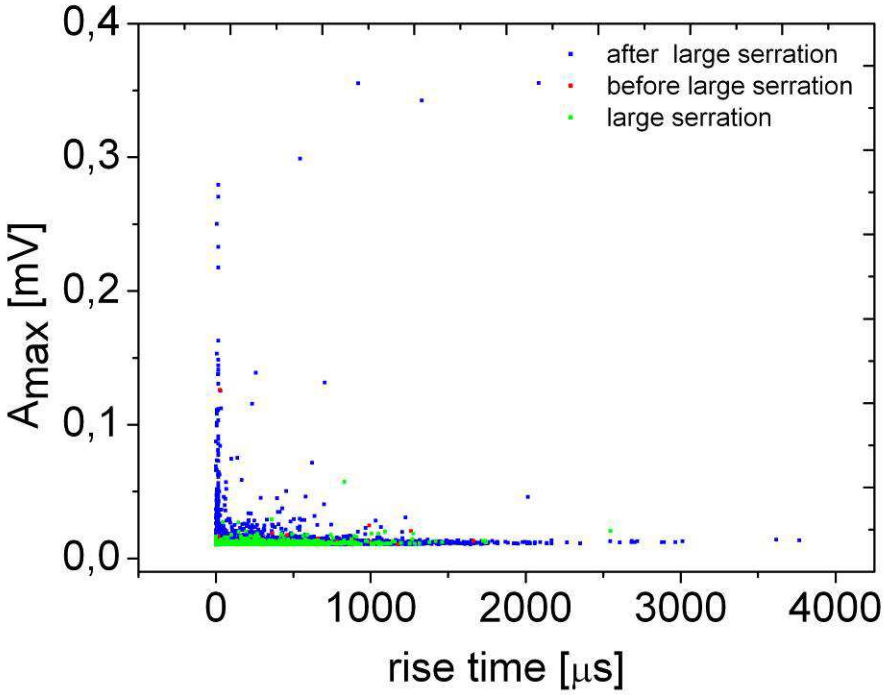

Fig. 48: The dependence of the A_{max} on the rise time of the AE events correlated with the deformation curve for the D10^{-4}s^{-1}4h530ºC specimen

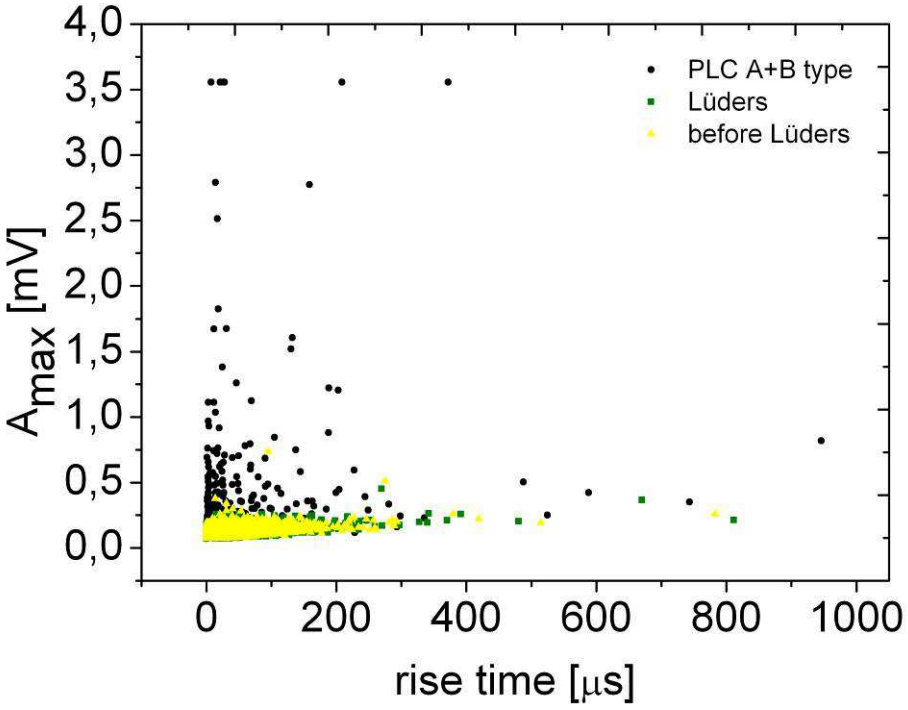

Fig. 49: The dependence of the A_{max} on the rise time of the AE events T10 $^{-3}$s^{-1}2h400ºC specimen of 5182 alloy

The figures show that AE events having a high A_{max} usually exhibit a short rise time and those with a low A_{max} can have a wide range of rise time. This is obvious for non-heat treated specimens. The D10^{-3}s^{-1}4h530ºC and D10^{-4}s^{-1}4h530ºC specimens (Fig. 47 and 48) which were heat treated for the longest time and deformed at the highest strain rate produced also AE events with an intermediate A_{max} and rise time at the same time. Fig. 49 shows the rise time dependence of A_{max} for 5182 alloy deformed in tension T10 $^{-3}$s^{-1}2h400ºC.

In Fig. 47 (specimen D10^{-3}s^{-1}4h530ºC) the A_{max} vs. rise time data are separated according time, when these events occurred. The AE events produced before the large serrations on the deformation curve have different A_{max} and rise time, but during the process, what caused the mean serration events with a short rise time occurred just as during the following area, where no main serrations, just small stress jumps were detected.

Fig. 48 (specimen D10^{-4}s^{-1}4h530ºC) shows the A_{max} - rise time dependence for the AE events determined from the area of the high stress jumps and from the area before and after these big serrations. It can be seen that concurrently with the

large stress jumps events with a very small A_{max} appeared just like before the large serrations. After this area events with a wide range of A_{max} and rise time were produced.

This separation of events was also performed for the T10 $^{-3}$s $^{-1}$ 2h400ºC specimen, which can be seen in Fig. 49. It shows, that AE events, which were detected before or during the Lüders phenomenon have similar parameters, both have small A_{max}. The events detected during the PLC effect had a large variety of A_{max} and rise time.

Discussion

The extrusion process is responsible for inhomogeneous distribution of precipitates in the investigated 6082 alloy and also for the elongation of grains into the ED. During the compression test, due to the local overstress, the grains elongated into ED (Fig. 5) deformed and therefore the final microstructure consists of equiaxial grains (see middle part of Fig. 5).

The microhardness of the selected specimens correspond with the preparation history of the investigated material. The as-received material has due to the production process and natural aging a relatively high dislocation density, which can be reduced with a help of heat treatment [11]. Lower Vickers microhardness values are observed in the deformed samples, which were heat treated ($D10^{-3}s^{-1}$4h530˚C∥, $D10^{-3}s^{-1}$4h530˚C⊥) in comparison to non-heat treated specimens ($D10^{-3}$∥, $D10^{-3}$⊥). The fact that the heat treatment duration does not influence the material hardness can be explained by a relatively high treatment temperature. At this temperature, the dislocations could annihilate during a short time and further heat treatment does not significantly influence the microstructure. The higher microhardness of the deformed comparing to non-deformed specimens is connected with increasing dislocation density during plastic deformation.

The slightly inhomogeneous Vickers microhardness of the deformed specimens ($D10^{-3}$, $D10^{-3}$4h530˚C), can be also seen from the standard deviation of the microhardness, presented in Table 5. Inhomogeneous deformation is represented by deformation bands in specimens, which causes the appearance of some areas with higher microhardness values.

The differences in the stress values for non-heat and heat treated specimens can also be related to various dislocation density at the beginning of deformation test. A higher dislocation density in non-heat treated specimens is caused by the production process and is responsible for higher stress values in comparison to heat treated specimens. Change in heat treatment time from 1 to 4 hours does not bring any differences in stress values.

The correlation of deformation curve with AE parameters opens a window for better description and understanding of dislocation dynamic in Al alloys exhibiting instable plastic deformation [20, 30, 34].

Plastic deformation in Al alloys is realized by a massive dislocation multiplication, especially at microscopic yield point, and by propagation and interaction of dislocations, which is an efficient AE source [3, 41]. During the compression tests after the elastic deformation of 6082 alloy, the PLC effect occurs, which causes serrations on the deformation curves. Since it is connected with the sudden motion of dislocation bands it produces AE events with a relatively low rise time [3, 40].

Non-heat treated specimens exhibit a less pronounced AE response than the heat treated specimens. It can be explained by the higher initial dislocation density and aged microstructure. In generally, increasing dislocation density reduces the flight distance and the free length of moving dislocations, which results in a decrease in the AE activity [29, 41]. Therefore, during the deformation only small dislocation groups could develop which were able to move small distances. This fact can also be used for explanation of low amplitude serrations on the deformation curves for non-heat treated specimens (Figs. 11-16).

Due to low initial dislocation density in heat treated specimens, their plastic deformation begins with massive dislocation multiplication [11]. Therefore, AE signals are determined as large AE events consisting from more overlapped AE events (Fig. 42 – D1). As a result, varying rise time for AE events during the experiment is detected. The different A_{max} and rise time values at the beginning and during the plastic deformation probably originate from this overlapping of more AE events. Due to high dislocation density at the end of the deformation, overlapping of AE events has a low probability to occur in this stadium of deformation (Fig. 42 – D2).

Correlation of serrations on the deformation curve with A_{max} can be influenced by overlapping of AE events. Not every deformation serration can be related to measurable AE response, because either the collective dislocation movement cannot produce detectable AE signals or strong AE signals due to overlapping of AE events can be observed as one. It follows that evaluation process in order to separate individual AE events is not adequate for all AE events (Fig. 42 – D1). By a modification of AE parameter values (increase of threshold level and minimum hit length, decrease of separation time, maximum hit length and dead time) a wave packet can be separated in incomplete AE events. On the other hand, such modification in values of AE parameters can cause a loss of small amplitude AE

events. This evaluation effect is also responsible for very high rise time which can be seen in Figs. 40 - 43.

The deformation curves of heat treated specimens exhibit pronounced serrations which are caused by their homogenized initial structure with a relatively low dislocation density. The low strain parts of deformation curves (Figs. 18, 21, 24 and 27) show large serrations containing small serrations. This can be explained by the motion of smaller dislocation avalanches before the motion of the whole dislocation band which also produces a detectable AE event [41], with a shorter rise time than it is produced by the motion of the whole band. Fig. 42– D1 shows how the AE events follow in the area where the serrated large stress jumps on the deformation curve were detected. The small amplitude AE events could be produced by changes which also caused the small serrations on the curve, whereas the last event on Fig. 42– D1, with the highest A_{max} could be caused by the same process (by the motion of the whole band) than the large stress jump on the deformation curve. This avalanche like character of dislocations bands movement was also observed in rise time *vs.* time plots (Figs. 40, 41 and 42) where a sequential increase in rise time values before a local maximum can be seen.

The high strain regions of deformation curves of specimens deformed at the highest strain rate (10^{-3} s^{-1}) show regularly serrated curves (Figs. 19 and 25). In this deformation state, the dislocation density can be so high [11] that only small separated dislocation avalanches can move what evokes to be a similar situation to non-heat treated specimens (Figs.12 and 13). Fig. 42– D2 shows an AE event produced almost at the end of the deformation which is probably caused by the PLC effect. The low rise time and the high A_{max} shows, that this burst signal is caused by the sudden motion of dislocation band.

The irregular serrations on the large stress jumps (Figs. 21 and 27) and in the region of the high strains (Figs. 22 and 28), observed for the heat treated specimens deformed at smallest strain rate (10^{-4} s^{-1}), can be explained by the longer waiting time of dislocation groups, caused by a slower increase of the local overstress at obstacles and by the motion of different dislocation groups. Similar scenario was also seen for non-heat treated specimens (Figs. 15 and 16).

In the case of the T10^{-3}2h400ºC specimen, at the beginning the low A_{max} and short rise time comes from the deformation of the preferably oriented grains. In the area of the Lüders phenomenon [40] the AE comes from the multiplication of the

dislocations. At the beginning of the specimen deformation the dislocation multiplication is so rapid that the AE events are detected as overlapped therefore the detected AE is continuous. Because of this events are evaluated as one event with a long rise time.

In the following area the PLC phenomenon occurs, causing burst AE events which are detected and evaluated as separated events, therefore there are high A_{max} and short rise time values [40].

During the deformation of materials, various processes can occur which have a different rise time and A_{max}. But these processes often have characteristic values which can be seen in Figs. 45-49 showing the dependence of the A_{max} on the rise time of the AE events.

At the beginning of the deformation of heat treated materials the dislocations multiply causing A_{max} and rise time dependent on the speed of the dislocation multiplication. In a structure deformed with high strain rate the dislocation multiplication is very rapid and the number of the dislocations which cause one AE event is higher than in a material deformed with a low strain rate. Since the dislocation density increases quickly, the AE events are detected as overlapped. The result is that in a fast deformed material the A_{max} is high due to the greater number of dislocations causing the event [30]. Similarly, because of the lower number of multiplied dislocations causing the AE event, the A_{max} is lower [30]. The rise time varies with the number of the overlapping events.

The AE events caused by the PLC effect, by the motion of the dislocation groups have a rise time and A_{max} dependent on the size of these moving dislocation groups and the applied strain rate. The large serrations are caused by the avalanche like movement of large dislocation groups. The smaller dislocation groups breaking away from the large dislocation band cause smaller serrations and AE events with smaller A_{max} but with a rise time dependent on the strain rate. In a material, deformed at high strain rate, the small dislocation groups can have a various number of dislocations but due to the high strain rate they will have a rather short rise time. In a material deformed at low strain rate these small dislocation groups would be pinned more effectively by solute atoms. Therefore the unpinned small dislocation group would have a very small A_{max} even if the event consists of overlapping events. But due to the overlapping of the events with different rise time the events will have a wide range of rise times.

At the end of the deformation, where no large serrations occur and the dislocation density is high [11], the high A_{max} event can come from the movement of large dislocation group or from degradation of material.

To study a possible occurrence of self-organised criticality in collective dislocation dynamic, power law distribution was used. The energy distribution of AE signals follows a power law which is given by $P(E_{AE}) \sim (A_{max}^2)^{-\alpha}$.

To check the influence of the parametrization of AE signals on results, various threshold voltages for determination of AE events were used (see also [42]). It can be seen that the power law exponent α is independent on its set up (Fig. 32). The main effect of increasing threshold voltage is in reduction of numbers of points in the dataset. The possible explanation for the data points which are below the linear dependence at low A_{max}^2 is the improper choice of the evaluation threshold value. When it is too close to the noise level, there are false detected AE events with small energies. The possible explanation for the data points which are above the linear dependence at low A_{max}^2 is the low value of the chosen bin size. Since most of the AE events have a small A_{max} the choice of a big bin size would result, that all these small A_{max} events would be counted in one group with a high $P(A_{max}^2)$. Decreasing the bin size the number of A_{max} events would decrease together with the $P(A_{max}^2)$.

The data point which is out of the linear dependence at high A_{max}^2 can be explained by the occurrence of AE signals which stem from massive internal changes, like cracking what results in enormous A_{max}. Since such events occur rarely, the evaluation program counts them into one group with a higher bin size, but the result is a high value of $P(A_{max}^2)$. In some cases, like in [44] data point occurred below the linear dependence. This deviation was in [43] explained as the effect of the internal stresses resulting from the restraint of an avalanche by grain boundaries.

Both investigated alloys show power-law distribution of A_{max}^2 over a range as long as 3 orders of magnitude independently on the alloys composition, parameters of deformation and microscopic processes which occur during plastic deformation. This confirms the hypothesis that the plastic deformation manifests a universal avalanche-type nature of the distribution of A_{max}^2. The variation of the exponent value with the deformation conditions shows that this exponent is not a universal value for all microscopic mechanisms of plastic deformation (see also [42]).

A similar finding has been published in [44]. It describes the results of compression creep experiments provided on ice single and polycrystals. In this work

a power law exponent $\alpha = 2.0 \pm 0.1$ was found for single crystals independently of the temperature confirming the independence of the critical dynamics of the individual dislocation behaviour. It argues that this result comes from the long-range elastic interaction between dislocations. In polycrystals a smaller power law exponent was found than in single crystals, which varied with the average grain size.

Different types of PLC serrations were observed during the compression tests. According to [14, 17] at the highest strain rate in the case of the non-heat treated specimen the D type occurred causing a deformation curve with repeating stress increase and plateau (Fig. 12). It was followed by a B type serration at high strains appearing as regular serration fluctuating about the stress-time curve (Fig. 13). In the non-heat treated material deformed with low strain rate in the small strain region a D type serration (Fig. 15) was observed which transformed in the high strain region into a C type serration fluctuating below the normal stress level (Fig. 16).The heat treated sample's serrated stress jumps for the highest strain rate can be named as type B (Figs. 18, 19, 24 and 25), but at lower strain rate the irregularly serrated curve has a C character (Figs. 21, 22, 27 and 28). During the tensile test a mixed A+B type PLC effect occurred (Fig. 31) [40].

Future work

The AE data streaming allows further analysis of detected AE signals. With the change of evaluation parameters (dead time, threshold voltage etc.) different AE events can be included into the statistical analysis of the results. It can help to study separately the AE events of different parameters. It also allows the separation of overlapped AE events.

The AE records as well as the deformation curves could be studied with the help of the multifractal analysis, which could reveal information about correlation between time or property scales [39,45].

Conclusions

Deformation tests were performed on 6082 and 5182 Al alloys with the concurrent detection of the AE signals. The experiments confirmed that the investigated specimens exhibit the PLC phenomenon which is manifested by serrations on the deformation curve. Moreover, 5182 alloy also exhibited the Lüders phenomenon, which occurred as serration on the deformation curve in the area of the plateau.

Different serration types were observed depending on the conditions of the deformation tests. In non-heat treated 6082 alloy, at high strain rates, the D type occurred followed by a B type serration and at small strain rates, the D type emerged following by a C type serration. During the deformation of the heat treated specimens at high strain rates the B type occurred and at lower strain rates, the serration had C character. During the deformation of the 5182 alloy the A+B mixed type was detected.

The change of the AE activity during the deformation was observed. In non-heat treated specimens, the AE activity was low, whereas in heat treated specimens high AE activity was detected during the multiplication of the dislocations and during the PLC effect.

With the help of the AE data stream the presence of the overlapped AE events during the AE evaluation was observed.

The independence of the power-law exponent on the choice of the threshold voltage used by the events extraction from the AE data stream was presented.

The power law distribution of $A_{max}{}^{2}$ was shown for all specimens with an exponent confirming the avalanche-like nature of plastic deformation.

With the help of clustering of the A_{max}-rise time dependence data, different processes which occurred during the deformations were distinguished and described.

Bibliography

[1] Z. Luo, A. Soria: *Prospective Study of the World Aluminium Industry*, JRC scientific and technical reports, Sevilla, 2007.

[2] J. Koutný: *Hliníkové materiály a možnosti jejich svařování*- available at www.svarbazar.cz (state as of 3.2.2014).

[3] A. Yilmaz: *The Portevin-Le Chatelier effect: a review of experimental findings*, Sci. Technol. Adv. Mater., 12, 2011, 1–16.

[4] B.J. Brindley: *The effect of dynamic strain-ageing on the ductile fracture process in mild steel*, Acta Metall. 18, 1970, 3, 325-329.

[5] *The New Encyclopaedia Britannica*, 15th ed., Chicago: Encyclopaedia Britannica, 1998.

[6] J. E. Hatch: *Aluminum: Properties and Physical Metallurgy*, ASM International, 1984.

[7] ČSN EN 573-1.

[8] The Aluminum Assocation, *Rolling Aluminum: From the mine through the mill*. 3rd ed., Arlington, 2007.

[9] ČSN EN 573-3.

[10] G. Mrówka-Nowotnik, J. Sieniawski, M. Wierzbiñska, *Intermetallic phase particles in 6082 aluminium alloy*, Mat. Sci. Eng., 28, 2007, 2, 69-76.

[11] P. Kratochvíl, P. Lukáč, B. Sprušil: *Úvod do fyziky kovů I.*, SNTL, Praha 1984.

[12] G. Ananthakrishna: *Current theoretical approaches to collective behavior of dislocations*, Phys. Rep., 440, 2007, 113–259.

[13] M.A. Lebyodkin, N.P. Kobelev, Y. Bougherira, D. Entemeyer, C. Fressengeas, T.A. Lebedkina, I.V. Shashkov: *On the similarity of plastic flow processes during smooth and jerky flow in dilute alloys*, Acta Mater. 60, 2012, 844-850.

[14] J. Balík, P. Lukáč: *Portevin-Le Chatelier instabilities in Al-3 Mg conditioned by strain rate and strain*, Acta Metall Mater, 41, 5, 1993, 1447-1454.

[15] K.G. Samuel, S.L. Mannan, P. Rodriguez: *Another Manifestation of Dynamic Strain Aging*, J Mater. Sci. Lett., 15, 1996, 167-1699.

[16] R.C. Picu: *A mechanism for the negative strain-rate sensitivity of dilute solid solutions*, Acta Mater., 52, 2004, 12, 3447-3458.

[17] E. Pink, A. Grinberg: *Serrated flow in a ferritic stainless steel*, Mater. Sci. Eng. 51, 1981, 1, 1-8.

[18] P. Rodriguez: *Serrated Plastic Flow*, Bull. Mater. Sci., 6, 1984, 4, 653-663.

[19] F. Chmelík, A. Ziegenbein, H. Neuhäuser, P. Lukáč: *Investigating the Portevin-Le Chatelier effect by the acoustic emission and laser extensometry techniques*, Mater. Sci. Eng. A 324, 2002, 200-207.

[20] Y. Bougherira, D. Entemeyer, C. Fressengeas, N. P. Kobelev, T. A. Lebedkina, M. A. Lebyodkin: *The intermittency of plasticity in an Al3%Mg alloy*, J. Phys.: Conf. Ser. 240, 2010, 012009.

[21] S. Cunningham: *Effect of substitutional elements on dynamic strain aging in steel*, Master Thesis, McGill University, Montreal, 1999.

[22] S.L. Mannan: *Role of dynamic strain aging on low cycle fatigue*, Mater. Sci., 16, 1933, 6, 561-582.

[23] Y. Brechet,Y. Estrin: *On the influence of precipitation of the Portevin-Le Charelier Effect*, Acta Metall. Mater., 43, 2006, 955-964.

[24] M. Abbadi, P. Hahner, A. Zeghloul: *On the characteristic of Portevin-Le Chatelier band in aluminum alloy 5182 under stress controlled and strain-controlled tensile testing*, Mater- Sci. Eng. A 337, 2002, 194-201.

[25] P. Dobroň: *Štúdium mechanických a fyzikálnych vlastností nových, konštrukčných materiálov na báze horčíka metodou akustickej emisie*, PhD thesis, MFF UK, Prague, 2007.

[26] M. Huang, L. Jiang, P.K. Liaw, Ch.R. Brooks, R. Seelev, D.L. Klarstrom: *Using acoustic emission in fatigue and fracture materials research*, JOM, 50, 1998, 1-12.

[27] I.G. Scott: *Basic acoustic emission*, Gordon and Breach Science Publisher, New York, 1991.

[28] J. Kaiser: *Untersuchungen über das Auftreten von Geräuschen beim Zugversuch*, PhD thesis, TU München, 1950.

[29] C.R. Heiple, S.H. Carpenter: *Acoustic emission produced by deformation of metals and alloys- A Review: Part I*, J.Acoustic Emission 6 ,1987, 177-204.

[30] C.B. Scruby, H.N.G. Wadley, J.E. Sinclair: *The origin of acoustic emission during deformation of aluminium and an aluminium-magnesium alloy*, Phil. Mag. A, 44, 1981, 249-274.

[31] C.R. Ríos-Soberanis: *Acoustic Emission Technique, an Overview as a Characterization Tool*, JART, 9, 2011, 367-379.

[32] *Standard Practice for Acoustic Emission Examination of Fiberglass Reinforced Plastic Resin*, ASTM E 1067-85. Tank/Vessels, May 31, 1985.

[33] P. Bak, C. Tang, K. Wiesenfeld: *Self-organized criticality: an explanation of 1/f noise*. Phys. Rev. Lett., 59, 381-384, 1987.

[34] M.A.Lebyodkin ,Y.Estrin: *Multifractal analysis of the Portevin–Le Chatelier effect: General approach and application to AlMg and AlMg/Al2O3 alloys*, Acta Mater., 53, 2005, 3403–3413.

[35] J.D. Farmer, J. Geanakoplosy: *Power laws in economics and elsewhere*, 2008 - available at imobbo.com/download/papers/Farmer-powerlaw3.pdf (state as of 3.2.2014).

[36] T. Richeton, P. Dobroň, F. Chmelik, J.Weiss, F. Louchet: *On the critical character of plasticity in metallic single crystals*, Mater. Sci. Eng. A, 424, 2006, 190-195.

[37] J. Weiss, J.R. Grasso, M.C. Miguel, A. Vespignani, S. Zapperi: *Complexity in dislocation dynamics: experiments* 2001, Mater. Sci. Eng. A, 309, 2001, 360-364.

[38] G. Ananthakrishna, S.J. Noronha, C. Fressengeas, L.P. Kubin: *Crossover from chaotic to self-organized critical dynamics in jerky flow of single crystals*
Phys. Rev. E, 60, 1999, 5455-5462.

[39] M.S. Bharathi, M. Lebyodkin, G. Ananthakrishna, C. Fressengeas, L.P. Kubin: *The hidden order behind jerky flow*, Acta Mater., 50, 2002, 2813- 2824.

[40] O. Molnárová: *Studium kolektivního chování defektů krystalové mříže metodou akustické emise*, Bachelor thesis, MFF UK, Praha 2012.

[41] K. Mathis, F. Chmelik: *Exploring Plastic Deformation of Metallic Materials by the Acoustic Emission Technique*, in: W. Sikorski (Ed.), Acoustic Emission, InTech, Rijeka 2012, 23–48.

[42] M.A. Lebyodkin, I.V. Shashkov, T.A. Lebedkina, K. Mathis, P. Dobron, F. Chmelik: *Role of superposition of dislocation avalanches in the statistics of acoustic emission during plastic deformation*, Phys. Rev. E 88, 2013, 042402.

[43] T. Richeton, J. Weiss, F. Louchet: *Breakdown of avalanche critical behaviour in polycrystalline plasticity*, Nat Mater, 4, 2005, 465-469.

[44] T. Richeton, J. Weiss, F. Louchet: *Dislocation avalanches: Role of temperature, grain size and strain hardening*, Acta Mater., 53, 2005, 4463-4471.

[45] M.A. Lebyodkin and T.A. Lebedkina: *Multifractal analysis of evolving noise associated with unstable plastic flow*, Phys. Rev., 73, 2006, 036114.

List of Tables

List of Abbreviations

a – final radius of the dislocation loops

AE – acoustic emission

$\vec{b}$ – Burgers vector of the dislocation

c_L – velocity of the longitudinal wave

CRSS – critical resolved shear stress

c_T – velocity of the transversal wave

d − the arithmetical average of the measured diagonals

D − specimen deformed in compression

DSA – dynamic strain aging

E_{AE} − energy of the acoustic emission event

F – the test force

fcc – face-centered cubic (lattice)

HV – Vickers hardness

K − constant

k − constant

A_{max} – the maximum amplitude of an AE event

n – number of the dislocation loops

$\dot{N}_C$ − acoustic emission count rate

$\dot{N}_E$ − acoustic emission event rate

N_C − cumulative acoustic emission count

N_E − cumulative acoustic emission event

PLC effect – Portevin- Le Châtelier effect

r – the distance of the dislocation source from the surface

RT – room temperature

SOC – self-organized criticality

SRS – strain rate sensitivity

t_d − dead time

t_e – the duration of the event

t_r − the rise time

t_s – the start time of the acoustic emission event

T – deformed in tension

ΔU – maximal amplitude of the surface shift in the epicentre

U_m − the total voltage

U_n − the noise voltage

U_r – the reference voltage

U_{RMS} − root mean square of the acoustic emission signal's voltage

v – velocity of the dislocation loop's growth

y – extenxion of the specimen

Z – signal amplification

α – the power-law exponent

ε – extension

$\vec{\zeta}$ – line element of the dislocation

$\sigma_{0,2}$ – offset yield strength

σ_m – ultimate strength

σ_y − yield strength

τ_0 − critical resolved shear stress